ENGINEERING OF BIOMATERIALS

INŻYNIERIA BIOMATERIAŁÓW

CZASOPISMO POLSKIEGO STOWARZYSZENIA BIOMATERIAŁÓW
I WYDZIAŁU INŻYNIERII MATERIAŁOWEJ I CERAMIKI AGH

Number 86
Numer 86
Volume XII
Rok XII

CZERWIEC 2009
JUNE 2009

ISSN 1429-7248

PUBLISHER:
WYDAWCA:

Polish Society for Biomaterials in Cracow
Polskie Stowarzyszenie Biomateriałów w Krakowie

ADDRESS OF EDITORIAL OFFICE:
ADRES REDAKCJI:

AGH-UST
30/A3, Mickiewicz Av.
30-059 Cracow, Poland
Akademia Górniczo-Hutnicza
al. Mickiewicza 30/A-3
30-059 Kraków

Issue: 200 copies
Nakład: 200 egz.

Scientific Publishing House AKAPIT
Wydawnictwo Naukowe AKAPIT
e-mail: wn@akapit.krakow.pl

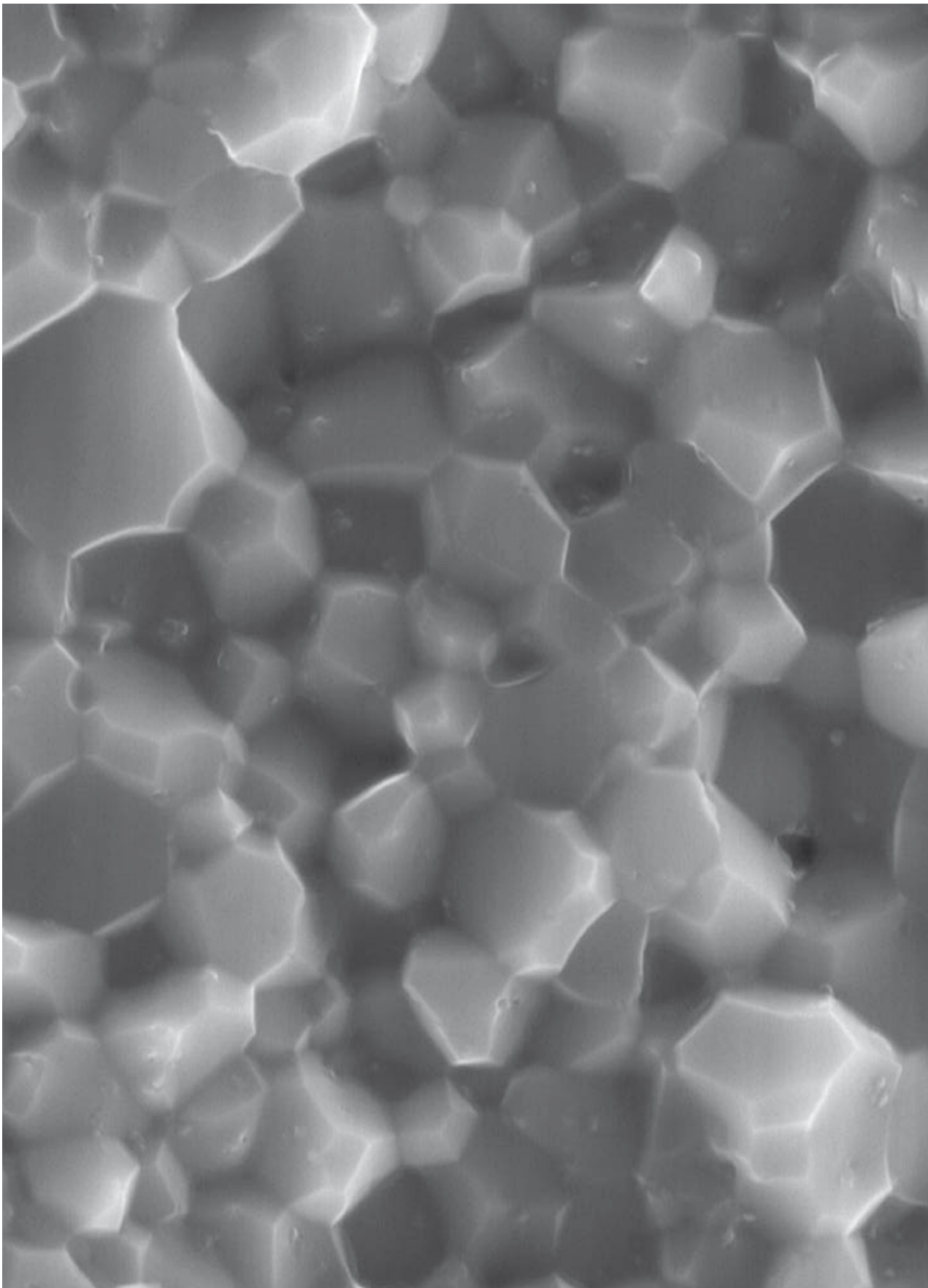

ENGINEERING OF BIOMATERIALS

INTERNATIONAL EDITORIAL BOARD
MIĘDZYNARODOWY KOMITET REDAKCYJNY

ENGINEERING OF BIOMATERIALS

Wskazówki dla autorów

1. Prace do opublikowania w kwartalniku „Engineering of Biomaterials / Inżynieria Biomateriałów" przyjmowane będą wyłącznie z tłumaczeniem na język angielski. Obcokrajowców obowiązuje tylko język angielski.
2. Wszystkie nadsyłane artykuły są recenzowane*.
(*Prace nierecenzowane, w tym materiały konferencyjne, będą drukowane w numerach specjalnych pod koniec roku kalendarzowego.)
3. Materiały do druku prosimy przysyłać na adres redakcji na płytach CD wraz z jednym egzemplarzem kontrolnego wydruku i kompletem rysunków i zdjęć lub na adres e-mail: kabe@agh.edu.pl
4. Struktura artykułu:
• TYTUŁ • Autorzy • Streszczenie (100-200 słów) • Słowa kluczowe • Wprowadzenie • Materiały i metody • Wyniki i dyskusja • Wnioski • Podziękowania • Piśmiennictwo
5. Materiały ilustracyjne powinny znajdować się poza tekstem w oddzielnych plikach. Rozdzielczość rysunków min. 300 dpi. Wszystkie rysunki i wykresy powinny być czarno-białe lub w odcieniach szarości i ponumerowane cyframi arabskimi. W tekście należy umieścić odnośniki do rysunków i tabel. W tabelach i na wykresach należy umieścić opisy polskie i angielskie. W dodatkowym dokumencie należy zamieścić spis tabel i rysunków (po polsku i angielsku).
6. Na końcu artykułu należy podać wykaz piśmiennictwa w kolejności cytowania w tekście i kolejno ponumerowany.
7. Redakcja zastrzega sobie prawo wprowadzenia do opracowań autorskich zmian terminologicznych, poprawek redakcyjnych, stylistycznych, w celu dostosowania artykułu do norm przyjętych w naszym czasopiśmie. Zmiany i uzupełnienia merytoryczne będą dokonywane w uzgodnieniu z autorem.
8. Opinia lub uwagi recenzenta będą przekazywane Autorowi do ustosunkowania się. Nie dostarczenie poprawionego artykułu w terminie oznacza rezygnację Autora z publikacji pracy w naszym czasopiśmie.
9. Za publikację artykułów redakcja nie płaci honorarium autorskiego.
10. Adres redakcji:

Czasopismo
„Engineering of Biomaterials / Inżynieria Biomateriałów"
Akademia Górniczo-Hutnicza im. St. Staszica
Wydział Inżynierii Materiałowej i Ceramiki
al. Mickiewicza 30/A-3, 30-059 Kraków

tel. (48 12) 617 25 03, 617 22 38
tel./fax: (48 12) 617 45 41
e-mail: chlopek@agh.edu.pl, kabe@agh.edu.pl
www.biomat.krakow.pl

Warunki prenumeraty

Zamówienie na prenumeratę prosimy przesyłać na adres:
apowroz@agh.edu.pl, tel/fax: (48 12) 617 45 41
Konto:
Polskie Stowarzyszenie Biomateriałów
30-059 Kraków, al. Mickiewicza 30/A-3
Bank Śląski S.A. O/Kraków,
nr rachunku 63 1050 1445 1000 0012 0085 6001
Opłaty: Cena 1 numeru wynosi 20 PLN

Instructions for authors

1. Papers for publication in quarterly magazine „Engineering of Biomaterials / Inżynieria Biomateriałów" should be written in English.
2. All articles are reviewed*.
(* Non-reviewed articles, including conference materials, will be printed in special issues at the end of the year.)
3. Manuscripts should be submitted to Editor's Office on CD with a printout, drawings and photos or by e-mail to kabe@agh.edu.pl
4. A manuscript should be organized in the following order:
• TITLE • Authors and affiliations • Abstract (100-200 words) • Keywords (4-6) • Introduction • Materials and methods • Results and Discussions • Conclusions • Acknowledgements • References
5. Authors' full names and affiliations with postal addresses should be given. If authors have different affiliations use superscripts 1,2...
6. All illustrations, figures, tables, graphs etc. preferably in black and white or grey scale should be presented in separate electronic files (format .jpg, .gif., .tiff, .bmp) and not incorporated into the Word document. High-resolution figures are required for publication, at least 300 dpi. All figures must be numbered in the order in which they appear in the paper and captioned below. They should be referenced in the text. The captions of all figures should be submitted on a separate sheet.
7. References should be listed at the end of the article. Number the references consecutively in the order in which they are first mentioned in the text.
8. Opinion or notes of reviewers will be transferred to the author. If the corrected article will not be supplied on time, it means that the author has resigned from publication of work in our magazine.
9. Editorial does not pay author honorarium for publication of article.
10. Papers will not be considered for publication until all the requirements will be fulfilled.
11. Manuscripts should be submitted for publication to:

Journal
„Engineering of Biomaterials / Inżynieria Biomateriałów"
AGH University of Science and Technology
Faculty of Materials Science and Ceramics
30/A-3, Mickiewicz Av., 30-059 Cracow, Poland

tel. (48 12) 617 25 03, 617 22 38
tel./fax: (48 12) 617 45 41
e-mail: chlopek@agh.edu.pl, kabe@agh.edu.pl
www.biomat.krakow.pl

Subscription terms

Subscription rates:
Cost of one number: 20 PLN
Payment should be made to:
Polish Society for Biomaterials
30/A3, Mickiewicz Av.
30-059 Cracow, Poland
Bank Slaski S.A. O/Krakow
account no. 63 1050 1445 1000 0012 0085 6001

XIX Conference on BIOMATERIALS IN MEDICINE AND VETERINARY MEDICINE

15-18 October 2009

Hotel "Perla Poludnia", Rytro

http://galaxy.uci.agh.edu.pl/~apowroz/biomat/

POLSKIE STOWARZYSZENIE BIOMATERIAŁÓW

PAN
POLSKA AKADEMIA NAUK

AGH

SPIS TREŚCI

CONTENTS

Streszczane w Applied Mechanics Reviews
Abstracted in Applied Mechanics Reviews

Wydanie dofinansowane przez Ministra Nauki i Szkolnictwa Wyższego
Edition financed by the Minister of Science and Higher Education

EFFECT OF MAGNETIC FIELD ON THE STRUCTURE FORMATION AND PROPERTIES OF HYDROXYETHYLMETHACRYLATE / POLYVINYLPYRROLIDONE COPOLYMERS

Oleg Suberlyak*, Volodymyr Skorokhoda

Lviv Polytechnic National University
Department of Chemical Technology of Plastics Processing
S. Bandera Str., 12, Lviv, 79013, Ukraine
* e-mail: suberlak@polynet.lviv.ua

Abstract

The effect of a permanent magnetic field on the polymerization kinetics and structural parameters of a hydrogel network on the basis of 2-hydroxyethylmethacrylate with polyvinylpyrrolidone compositions has been investigated. It has been shown that the magnetic field activates matrix polymerization of mentioned compositions and assists in the structure formation of copolymers with a smaller crosslink density. The efficiency of the developed polymeric materials for production of ultrathin contact lenses "Glipox" has been confirmed.

Keywords: *polyvinylpyrrolidone, 2-hydroxyethylmethacrylate, magnetic field, matrix polymerization*

[Engineering of Biomaterials, 86 (2009), 2-4]

Introduction

The polyvinylpyrrolidone (PVP) / 2-hydroxyethylmethacrylate (HEMA) cross-linked copolymers are successfully applied in biomedical practice, including the manufacture of endoprostheses, contact lenses, implants, dental compositions etc. [1]. They are obtained, basically, via thermo-, photo- and radiation polymerization in the presence of initiators or without them [2,3]. The main regularities of such syntheses and reactions topological schemes were developed at the Department of Chemical Technology of Plastic Processing of the Lviv Polytechnic National University; the possibility of polymerization process activation both under homogeneous conditions and on the phase boundary has been revealed as the result of the charge-transfer complex formation into the system of monomer – polymeric matrix – protophobic solvent.

It is foreseen that under polymerization the reactivity of polymeric matrix may be strengthened by orientational, diffusive and solvation effects generated by external energy fields, permanent magnetic field in particular. At the same time the polymerization processes under the influence of the magnetic field (MF) have not been studied thoroughly, though they are important both from scientific and practical points of view. Therefore, the researches in this direction foresee the deepening of theoretical conceptions about polymer formation and enhancement of possibilities for synthesis of new polymers and modification of existing ones resulting in the new non-traditional syntheses of perspective hydrogel materials on the basis of PVP copolymers.

Aim of the work

The aim of this work is to investigate the effect of the permanent magnetic field on the polymerization kinetics, structure formation and properties of HEMA / PVP copolymers.

Materials and methods

HEMA (Bisomer) used for polymerization was purified by vacuum distillation (residual pressure is 130 N/m^2, T_{boil} = 351 K). Also ethylene glycol dimethacrylate (DMEG; Merck) (T_{boil} = 343 K under the residual pressure of 400 N/m^2) and high purified polyvinylpyrrolidone (PVP; AppliChem GmbH) with mol. wt. $28 \cdot 10^3$ were used. Benzoyl peroxide (BP), having been recrystallized twice from methanol, was used as the initiator of polymerization.

The permanent magnetic field was created by the powder magnets "Niomax" on the basis of ferrum-neodymium-boron $Fe_{14}Nd_2B$ which were characterised by the following properties: the residual magnetic induction, B_r = 1.15 T; the coercive force on magnetization, jH_c = 400 kA/m; the maximum magnetic energy, $(BH/2)_{max}$= 240 kJ/m^3. Magnets had the form of disks with a diameter of 97 mm and thickness of 20 mm which were clasped by magneto-conductor with one mobile pole. The intensity of magnetic field was regulated by a free clearance between disks.

Structural parameters of the polymeric net in hydrated state were estimated by means of the molecular weight of macrochain section (M_n) between neighboring cross-linking nodes or by means of cross-linking density ($v = 1/M_n$) determined using module of high elasticity.

The molecular weight of chain section between neighboring cross-linking nodes was calculated by the following formula [4]:

$$M_n = \frac{L^5 \rho_p v_s}{0{,}5 - \mu},$$

where:
L – coefficient of linear swelling;
ρ_p – polymer density, kg/m^3;
v_s – molar volume of the solvent, m$^3 \cdot$kg$^{-1} \cdot$mol^{-1};
μ – parameter of polymer-liquid interaction

$$\mu = 0{,}5 - \frac{\nu_s \sigma_\infty L^4}{RT(\lambda^2 - \lambda^{-1})},$$

σ_∞ – equilibrium tension, kgf/m^2

$\lambda = 1 + \varepsilon, \quad 0 < \varepsilon < 0{,}3,$

ε – equilibrium tension strain.

Polymerization kinetics was investigated using dilatometric analysis [5], composition of copolymers were investigated by the procedures described in [6] and permeability of polymers for water and NaCl was investigated by the procedure offered by Karelin [7].

Results and discussion

HEMA polymerization was studied in the presence of PVP at the ratio HEMA:PVP = 10:0...7:3 weight parts (wt.p.) in the range of magnetic field intensity H = 0...310 kA/m and temperatures 303...333 K. The influence of MF on homopolymerization kinetics of HEMA was studied previously at the ratio monomer : initiator = 10:0,03 wt.p. at 313 K. It was determined that homopolymerization of HEMA both in a magnetic field, and without it proceeds with the same rate (FIG. 1, curve 5 and 5´), i.e. it is possible to ascertain that MF does not influence the HEMA homopolymerization.

At the same time, MF accelerates polymerization in the case of PVP-containing compositions with peroxide as well as without it. The polymerization rate increases proportionally to the increase of polymeric matrix amount in the composition, the same as for thermoinitiated polymerization (FIG. 1).

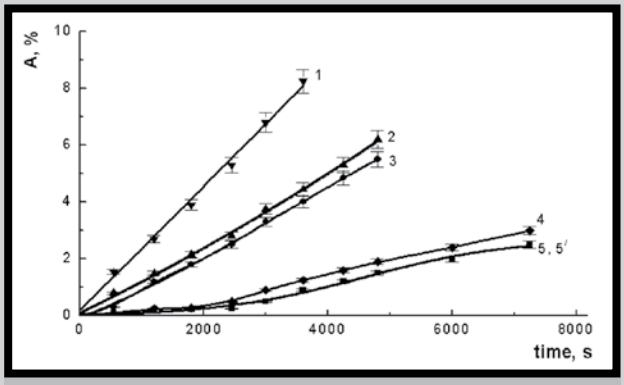

FIG. 1. Dependence of polymer A yield upon mixture composition.
[PB] = 0.3%. HEMA:PVP mixture composition, wt. p.: 1 - 7:3; 2 - 8:2; 3,4 - 9:1; 5,5' - 10:0; MW_{pvp} = 28000; Intensity of magnetic field H, кА/м: 1...3, 5 - 310; 4, 5' - 0; T = 313 K.

The mentioned phenomena may be explained using previously determined mechanism of matrix polymerization of (meth)acrylates in the presence of PVP. The process evidently is accompanied by monomer molecules salvation over PVP-matrix with the charge-transfer complex formation [8] (SCHEME 1).

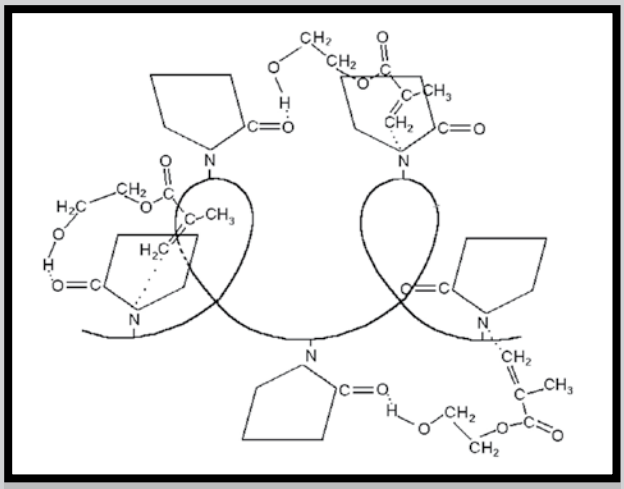

SCHEME 1. Complexation between HEMA and PVP.

The dissociation of double bond in monomer molecules is facilitated and the polymerization rate increases due to the complex formation. On the other hand, probably [9], the orientation in the magnetic field is caused, mainly, by the anisotropy of molecules diamagnetic susceptibility. The single bond has the greatest diamagnetic susceptibility when the field is directed along a bond axis; therefore the molecule is orientated perpendicularly to a field. On the contrary, the double bond has the greatest value when the field is directed perpendicularly to a bond axis and the molecule is orientated in parallel to the magnetic field. In the article [9] it was supposed that the peptide bond should have the anisotropy of a diamagnetic susceptibility because it partially has the character of the double bond due to the presence of two resonance structures. Thus, the peptide bond anisotropy has the same sign and almost the same value as the double bond.

Taking into account all above mentioned and the similarity of the peptide bond with the bond in the PVP macromolecule, it is possible to foresee that the plane of the single bond in the PVP macromolecule tends to be oriented perpendicularly to MF, and the bond connecting a cycle with the main chain is parallel to MF(as well as the plane of the double bond C=C in the monomer) (SCHEME 2).

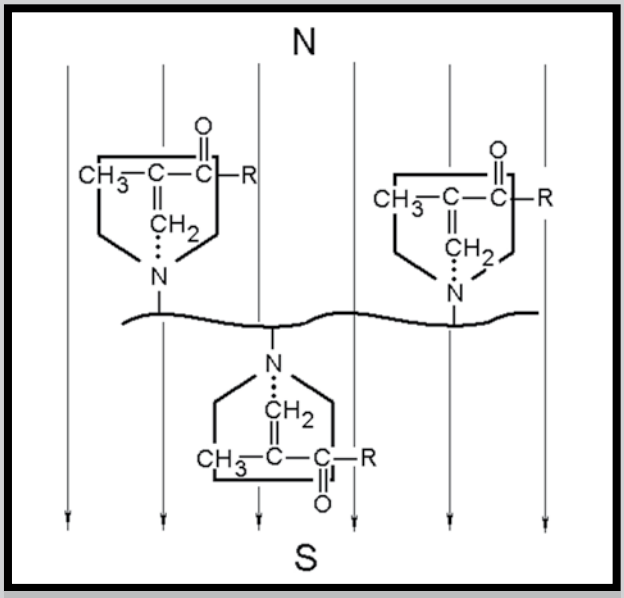

SCHEME 2. The components orientation of monomer-polymer composition in MF.

Also it is possible to foresee that aggregation of monomer molecules near the polymeric matrix would be easier owing to such orientation under MF influence. This fact, in turn, facilitates the access of monomer molecules to the active groups of PVP macromolecules strengthening in such a way the complexation, which is the factor of polymerization acceleration [8]. As a result of the oriented placing of macromolecules the mobility of formed associates decreases, the best kinetic conditions of chain growth are created, and also the initial conditions of the structure formation of (co)polymers with the arranged distribution of macrochains are established.

During polymerization in the solution the nature of a solvent and its properties, among which dielectric constant (ε) is the determining factor, have the great influence on the polymerization rate (TABLE 1). The researches have shown that the polymerization rate of the HEMA / PVP compositions decreased in the following row: water (ε = 78.3) > dimethyl sulfoxide (DMSO) (ε = 46.6) > ethylene glycol (EG) (ε = 37.7) > butanol (ε = 17.7).

TABLE 1. Effect of magnetic field intensity (H) and solvent dielectric constant (ε) on the polymerization rate (V) of compositions with PVP (T = 313 K).

№	Composition *	H, кА/m	ε	V, mol·dm^{-3}·s^{-1}
1	HEMA:PVP	0		$4.7 \cdot 10^{-5}$
2		310		$11.4 \cdot 10^{-5}$
3	HEMA:PVP:H_2O	310	78.3	$8.8 \cdot 10^{-6}$
4	HEMA:PVP:DMSO	310	46.6	$5.2 \cdot 10^{-6}$
5	HEMA:PVP:EG	310	37.7	$2.3 \cdot 10^{-6}$
6	HEMA:PVP:butanol	310	17.7	$1.3 \cdot 10^{-6}$
* – HEMA:PVP: solvent :PB = 9:1:10:0,02 wt. p.				

TABLE 2. Structural characteristics of the net and properties of copolymers synthesized in MF (T = 313 K, [PB] = 0.3 mas.%).

HEMA:PVP, wt. p.	MF intensity, κA/m	M_n, kg·mol^{-1}	v=10^2/M_n, mol·kg^{-1}	$D_{NaCl}\cdot10^{12}$, m^2/s	F*, MPa	T_V*, K
10 : 0	0	6.2±1.0	16.1	0.83	200±5	357±1
	310	17.3±2.0	5.8	0.94	278±5	378±2
9 : 1	0	7.0±1.0	14.3	0.89	219±5	365±1
	310	9.5±1.0	10.5	1.00	258±5	377±1
8 : 2	0	11.3±1.0	8.9	2.11	288±5	369±1
	310	11.9±1.5	8.4	2.61	333±8	383±2
7 : 3	0	11.7±1.5	8.6	3.49	296±7	372±1
	310	14.6±1.5	6.9	4.17	340±8	385±2

M_n - molecular weight of the net fragment; v - cross-linking density; D_{NaCl} - coefficient of NaCl diffusion through the hydrogel; F - surface hardness; T_V - heat resistance by Vicata,
* - properties in the solid state, others - in the equilibrium swelling state.

On the basis of experimental investigations the basic kinetic parameters of the polymerization reaction (rate constants, reaction orders, activation energy) for the composition HEMA:PVP = 9:1 wt.p. in MF have been calculated. The effective activation energy of the process in DMSO is 46 ± 2, in water – 39 ± 2 kJ/mol. These values are considerably lower in comparison with polymerization of such systems without MF (67 and 57 kJ/mol, respectively). The received values testify the active role of solvents in the polymerization process in MF, with changes depending on their dielectric constant.

At the same time, it has been established that MF essentially influences the crosslinking during HEMA homopolymerization. In the MF crosslinking density considerably decreases compared with polymerization of PVP-compositions (TABLE 2), though MF practically does not affect the homopolymerization kinetics of HEMA.

The obtained dependences correlate with above mentioned orientation scheme of the components of monomer-polymeric composition in the magnetic field and are caused by MF effect on the aggregation of monomer molecules due to the polarising and orientational phenomena. Since the planes of C=C double bonds of HEMA, as well as of ethylene glycoldimethacrylate (DMEG) which is responsible for the formation of the structural network at HEMA polymerization are oriented in parallel to the external magnetic field, the best kinetic conditions of chain growth in the reaction of binary copolymerization of HEMA with DMEG are created. Therefore the part of the latter component decreases in crosslinking reaction and copolymer with less crosslinking density (higher value of Mn) and the better operational properties is formed (TABLE 2).

The copolymers operational properties and their interdependence with the structure and obtaining conditions have been examined in order to develop the synthesis technology for the production of medical wares, including contact lenses. It has been established that MF with the intensity of 310 kA/m increases sorption ability by 10…15 % and permeability of copolymers for water and soluble low-molecular substances (TABLE 2), which is one of the basic characteristics for estimation of duration and ophthalmic comfort of the lenses. The increase of surface hardness of the synthesised in MF copolymers (which determines their fitness for mechanical treatment) compared with those obtained via thermopolymerization (from 200 to 278 MPa for homopolymer and from 210...296 to 231...340 MPa for copolymers depending on their composition), is determined by the fact that under MF conditions the polymer with a more ordered and less defective structure is formed. The researches have confirmed the possibility to obtain hydrophilic polymers with the increased physico-mechanical properties in the constant MF with the following mechanical treatment.

The results of the investigations concerning the MF effect on the structure formation of copolymers have been used to obtain hydrophilic polymers necessary for production of ultrathin contact lenses “Glipox” and accommodative crystalline lenses. The properties of the “Glipox” material are given in TABLE 3.

The lenses have successfully passed the industrial and toxicological tests. They are stable to the action of detergents and disinfectants and stand sterilization in water without changing their optical and physico-mechanical properties. The lenses are produced with a refraction from – 25 to +18 D, the thickness in the centre – from 0.04 to 0.10 mm depending on the refraction. Thus it is necessary to pay attention to the important property of lenses to keep the form without curling and high optical properties even at the least thickness.

TABLE 3. Technical characteristics of the contact lenses “Glipox” in equilibrium swelling state.

Technical features and its value	Value
Minimal thickness of the lens in the centre, mm	0.04
Tenacity, MPa	6.9
Elasticity, %	69
Water content, %	38
Permeability of light, %	96
Permeability* of NaCl, mol·m^{-2}·h^{-1}	264
* Permeability* of water, m^3·m^{-2}·h^{-1}	76.3·10^{-3}
* − for minimal thickness	

Conclusion

It has been determined the active effect of permanent magnetic field on the polymerization kinetics of HEMA / PVP compositions and the formation of more ordered structure of copolymers with less crosslinking density and better properties. It has been used for technological implementation of polymeric material “Glipox” used for ultrathin contact lenses.

References

[1] Suberlyak O., Skorokhoda V., Gavlo I. Copolymers of polyvinylpyrrolidone and products for medicine. Plastics in Machine Design, Kraków (1997) 419-422.
[2] Skorokhoda V., Semenyuk N., Suberlyak V. Structure and sorption ability of oxyethylenmethacrylate and PVP copolymers. Polimernyj Zhurnal 2 (2004) 86-91.
[3] Suberlyak O., Skorokhoda V., Levitsky V. The effect of phase boundary on polymerization of vinyl monomers in the presence of polyvinylpyrrolidone. Ukr. Polymer Jornal 1-2 (1995) 177-185.
[4] Shvarc A, Grigorovskaya V. At the question about value of link crossing concentration. Colloid Journal 1 (1985) 30-34.
[5] Yacymmirskiy K. Kinetic methods of analysis. Moscow: Chimiya 1972.
[6] Suberlyak O., Skorokhoda V., Grytsenko O. Complex PVP-Me^{n+} - active catalyst of vinyl monomers polymerization. Materialy Polimerowe i Ich Przetworstwo. Czestochowa 2004,140-145.
[7] Dubyaga V., Perepechkin L., Katalevskiy E. Polymers Membranes. Moscow: Chimiya 1981.
[8] Suberlyak O., Skorokhoda V., Tkhir I. Complex formation effect on the HEMA polymerization at the PVP presence. Vysokomolekul. soed. 5 (1989) 336-340.
[9] Ivanov B. Magnetic spin effects at the polymers synthesis. Vysokomolekul. Soed. 9 (1991) 1811-1827.

FORMATION AND PROPERTIES OF HYDROGEL MEMBRANES BASED ON CROSS-LINKED COPOLYMERS OF METHACRYLATES AND WATER-SOLUBLE POLYMERS

Oleg Suberlyak*, Joury Melnyk, Volodymyr Skorokhoda

Lviv Polytechnic National University,
Department of Chemical Technology of Plastics Processing
S. Bandera Str., 12, Lviv, 79013, Ukraine
* e-mail: suberlak@polynet.lviv.ua

Abstract

Experimental results concerning the effect of composition, nature of polymeric matrix, monomer and solvent on the structure, physico-mechanical and selective-transport characteristics of hydrogel membranes based on cross-linked grafted copolymers of methacrylates and water-soluble polymers (polyvinylpyrrolidone, polyvinyl alcohol) have been presented. Methods of high-penetrating hydrogel membranes formation have been developed and capability of directional control of their structure and operational characteristics has been determined.

Keywords: *hydrogels, methacrylates, polyvinylpyrrolidone, polyvinyl alcohol, permeability*

[Engineering of Biomaterials, 86 (2009), 5-8]

Introduction

Cross-linked grafted copolymers of methacrylates and functionally active polymers, polyvinylpyrrolidone (PVP) and polyvinyl alcohol (PVA) in particular, are widely used in medicine due to their valuable properties. The main area of application is production of contact lenses, biologically compatible implants, membranous drugs, membranes for biological compounds concentration and purification, systems of drug release, etc. [1,2]. Such materials form polymeric hydrogels after water sorption. It is well-known that hydrogel properties are determined by the chemical structure and structural parameters of their net. Therefore, in this paper we have investigated the effect of composition and formation conditions on the structure and properties of cross-linked hydrogel membranes based on PVP and PVA copolymers with methacrylates.

Materials and methods

Synthesis of hydrogel membranes and study of their compositions were carried out in accordance with previously developed procedure [3]. 2-Hydroxyethyl methacrylate (HEMA; Bisomer) and glycidyl methacrylate (GMA; Mitsubishi Rayon Co. Ltd) were used as monomers. Both HEMA and GMA were purified and distilled under vacuum: residual pressures were 130 and 520 N/m^2 and boiling temperatures were 78 and 69°C, respectively. High-purified PVP (AppliChem GmbH) with molecular weight of $10 \cdot 10^3$ and PVA (Gohsenol) with acetate groups content 0.8-2.0% were used as polymeric matrices. Polymerization was initiated by potassium persulphate and isopropylbenzene hydroperoxide.

Hydrogel membranes were obtained by combining the membrane formation stage and composition polymerization stage in the solution of one or more solvents (mostly in water) or by hardening the composition in the formed membranous net after solvent evaporation. Before the experiments membranes were hydrated in water until the equilibrium state was achieved.

Structural parameters of the polymeric net in hydrated state were estimated by means of the molecular weight of macrochain section (M_n) between neighboring cross-linking nodes determined using module of high elasticity.

The molecular weight of chain section between neighboring cross-linking nodes was calculated by the following formula [4]:

$$M_n = \frac{L^5 \rho_p v_s}{0{,}5 - \mu},$$

where:
L – coefficient of linear swelling;
ρ_p – polymer density, kg/m^3;
v_s − molar volume of the solvent, m$^3 \cdot$kg$^{-1} \cdot$mol^{-1};
μ – parameter of polymer-liquid interaction

$$\mu = 0{,}5 - \frac{v_s \sigma_\infty L^4}{RT(\lambda^2 - \lambda^{-1})},$$

σ_∞ – equilibrium tension, kgf/m^2

$\lambda = 1 + \varepsilon, \quad 0 < \varepsilon < 0{,}3,$

ε – equilibrium tension strain.

Sorption characteristics of obtained hydrogel membranes were determined using a gravimetric method. Mechanical properties were determined using a break method, by means of specially constructed device “Kimura Machinery” of 050/RT-6010 type, according to the procedure presented in [5]. This device allows to carry out investigations in aqueous medium. Diffusive permeability of synthesized membranes for water and model substance soluble in it (sodium chloride) without external pressure is determined using laboratory osmometer according to the procedure suggested by Karelin [6]. Effectiveness and inhibitory action for salt aqueous solutions at ultrafiltration were determined using FM-02 laboratory plant, being pressurized by air supplied from a compressor. The change of salt concentration in the solution was estimated by filtrate conductivity using P577 measuring bridge with platinum reference electrodes.

Membrane effectiveness by filtrate (J, m$^3 \cdot$m$^{-2} \cdot$h^{-1}) at ultrafiltration is determined by the following formula [7]:

$$J = \frac{\Delta Q}{S \cdot \Delta \tau},$$

where ΔQ is volume (m^3) of filtrate penetrating through the membrane with area S (m^2) for time τ (h).

Inhibitory action for salts (R_z) is calculated by the following formula:

$$R_z = \frac{C_0 - C_f}{C_0} \cdot 100\%,$$

where C_0, C_f are salt concentrations in the initial solution and filtrate, respectively, mol/l.

Results and discussion

Investigations of physico-mechanical properties of synthesized hydrogel membranes show that the presence of PVA in their structure, when copolymer (PVA-HEMA) contains regularly allocated hydroxyl groups of high-molecular fragments and alkoxyl branching, considerably improves deformation-strength characteristics (strength and elasticity increase, TABLE 1) compared with membranes, where hydroxyl groups of high-molecular fragments are changed

for pyrrolidone cycles with ionogenic groups (–NCO) of PVP macromolecules, as well as with known polyHEMA membranes [8] only with alkyl branching. The high mechanical strength of membranes based on PVA is caused, to our mind, by intermolecular interaction inside polymeric matrix due to hydrogen bonds between regularly allocated hydroxyl groups [9].

During membranes synthesis the change of water part for dimethylsulphoxide (DMSO) increases internodal molecular weight of hydrogel net which should increase their permeability. At the same time hydrogels' mechanical properties do not change (0.45 and 0.49 MPa, TABLE 1). Thus, introducing aprotonic DMSO into the initial composition we can directionally regulate the structural parameters of hydrogel net and change penetrability of the membrane on its basis in the necessary direction.

Membranes based on PVA-PVP-HEMA combined polymeric matrix are characterized by less net density (higher M_n) compared with those based on polyHEMA [8] and PVA-HEMA (TABLE 1). However, mechanical strength of these membranes is relatively low (0.4-0.5 MPa), which essentially constricts possibilities of their application in baromembrane processes. The increase of PVP content, as well as the decrease of HEMA concentration in membranes based on PVA-PVP-HEMA combined polymeric matrix, result in the decrease of their mechanical strength (TABLE 1, pos. 2, 4) though the molecular weight of internodal fragment is the same.

In order to increase the mechanical strength of hydrogel membranes we investigated the possibility of introducing GMA, soluble in DMSO, into the initial composition. It has been established that GMA introduction (TABLE 1, pos. 6) slightly decreases the net density and increases mechanical characteristics twice.

Investigations confirm that the nature of polymeric matrix and initial monomer have an essential effect on the structural parameters of hydrogel net (M_n) (TABLE 1). However, for all PVA-containing membranes water content is approximately the same (TABLE 2).

We have established that permeability of synthesized hydrogel membranes during the processes without external pressure (osmosis) does not depend directly upon material water content and net structural parameters, i.e. the increase of water content and internodal molecular weight do not cause the identical increase of coefficients of water- (K) and salt-osmotic (α) permeability (TABLE 2). Apparently, in such a case conformational transformations and polarization of copolymer functional groups with appearance of a surface charge play the important role. The membranes based on PVA-PVP-HEMA combined polymeric matrix are characterized by higher osmotic water permeability compared with those based on PVA-HEMA and especially with membranes based on polyHEMA (TABLE 2).

It is known that in membranous processes the factors favorable to hydrogel polymeric net opening stimulate the decrease of strength on the one hand and the increase of water content with corresponding increase of hydrogel membranes effectiveness on the other hand [9]. We have established that in filtration processes synthesized membranes effectiveness increases with the increase of applied external pressure. Therefore for investigations of transport-selective characteristics in ultrafiltration processes we have chosen membranes with the structure ensuring regular and gradual change of effectiveness upon the pressure within the range from 0 to 2 kgf/cm^2.

The effect of pressure on the hydrogel membranes effectiveness by distilled water has been examined. For all membranes based on PVA and PVP the increase of applied pressure causes the increase of effectiveness by water.

TABLE 1. Physico-mechanical properties of hydrogel membranes in hydrated state.

No	Composition of forming solution, wt. parts				M_n, kg/mol	Tensile strength, σ_t, MPa	Relative elongation at rupture, ε_r, %
			HEMA	H_2O			
1.	–	30	30	200	15	10,5	500
2.	25	5	30	200	175	0,29	281
3.	25	10	30	200	180	0,45	390
4.	30	15	15	200	185	0,21	260
5.	25	10	30	200 DMSO	195	0,49	295
6.	25	10	15+15 GMA	100 + 100 DMSO	146	0,87	510
M_n is molecular weight of net internodal fragment							

TABLE 2. Sorption-diffusive characteristics of hydrogel membranes (thickness 30 μm).

No	Composition of forming solution, wt. parts				Water content, W, %	Coefficient of permeability	
	PVA	PVP	HEMA	H_2O		by water $K \cdot 10^4$, $m^3 \cdot m^{-2} \cdot h^{-1}$	by NaCl α, $mol \cdot m^{-2} \cdot h^{-1}$
1.	30	–	30	200	84	52	404
2.	5	25	30	200	75	150	320
3.	10	25	30	200	80	280	320
4.	15	30	15	200	81	280	437
5.	–	–	100	100	40	5	80

Moreover, if under small pressures (0.2-0.6 kgf/cm^2) there is minimum dependence of effectiveness upon pressure, the pressure differential more than 0.6 kgf/cm^2 leads to the exponential increase of effectiveness (FIG. 1). Apparently, the optimum orientation of polymeric chains in the direction of pressure effect with the formation of a channel type structure with a minimum resistance to a liquid flow takes place.

The effect of mixture structure on the membranes permeability has been established. In particular, at ultrafiltration processes the change of water part for DMSO under low pressures (till 1 kgf/cm^2) also increases the effectiveness of synthesized hydrogel membranes (FIG. 1).

The results of investigations concerning the effect of the mixture structure upon hydrogel membranes effectiveness by water confirm the possibility of their application as ultrafiltration membranes. Moreover, the change of a solvent composition allows to change their effectiveness under ultrafiltration pressures higher than 0.6 kgf/cm^2. We may conclude that membranes based on combined matrix PVA and PVP are sufficiently strong, they can withstand the pressure differential till 2 kgf/cm^2 and may be used in baromembranous separation processes from aqueous solutions.

The transport-selective characteristics of synthesized hydrogel membranes have been investigated in ultrafiltration processes of model substances – electrolytes of different nature: NaCl, $CaCl_2$ and Na_2SO_4. Transport properties of synthesized hydrogel membranes have a complicated character. Their high elasticity does not prevent ultrafiltration: at the pressure differential prior to 0.2 kgf/cm^2, the process is not accompanied by deformation of membranes porous structure and their effectiveness by water increases with the increase of applied pressure (FIG. 2).

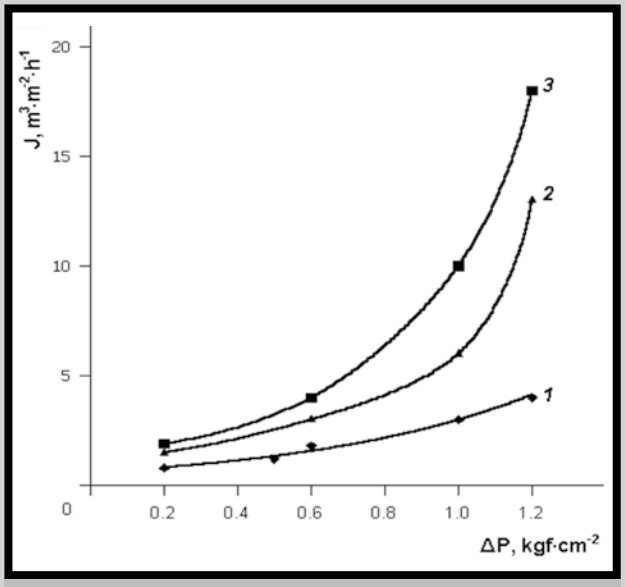

FIG. 1. Dependence of hydrogel membranes effectiveness by water (J) upon pressure differential (ΔP) (δ = 30 μm).
Composition of forming solution, wt. parts:
1 – PVA:PVP:HEMA:H_2O = 10:25:30:200;
2 – PVA:PVP:HEMA:GMA:H_2O:DMSO = 10:25:15:15:100:100;
3 – PVA:PVP:HEMA:DMSO = 10:25:30:200.

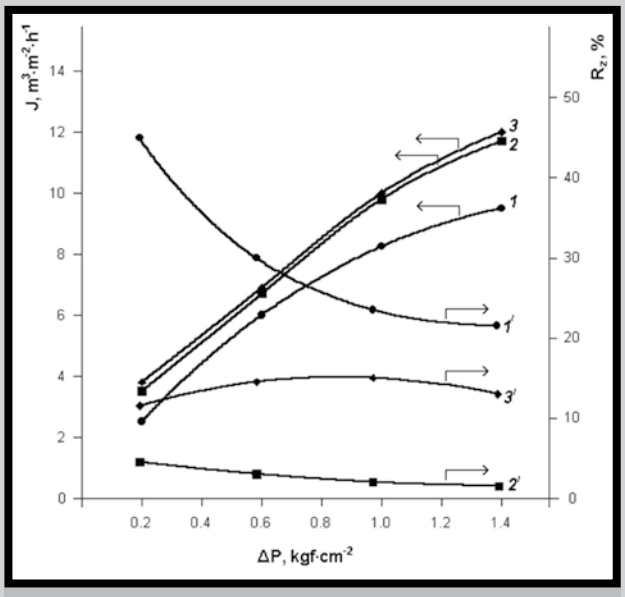

FIG. 3. Dependence of effectiveness by filtrate (J) and inhibitory action (R_z) upon pressure differential (ΔP) at ultrafiltration of salt solutions for hydrogel membranes based on PVA-PVP-HEMA (δ = 30 μm).
C_{salt} = 0,1 mol/l; 1, 1′ – NaCl; 2, 2′ – $CaCl_2$; 3, 3′ – Na_2SO_4.

At the same time there is a specific property of synthesized hydrogel membranes - the inhibitory action takes place at ultrafiltration of low-molecular substance solutions (FIG. 2). This fact contradicts to some extent with structural-steric concepts taking into account the ratio between ion and molecule sizes and structural parameters of polymeric matrix net (M_n), as well as high values of water content of synthesized hydrogels.

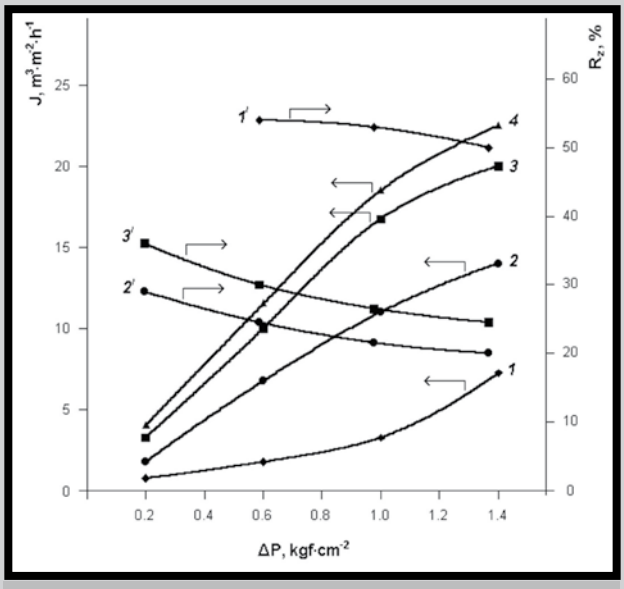

FIG. 2. Dependence of effectiveness by filtrate (J) and inhibitory action (R_z) upon pressure differential (ΔP) at ultrafiltration of salt solutions for hydrogel membranes based on PVA-HEMA (δ = 30 μm).
C_{salt} = 0,1 mol/l; 1, 1′ – Na_2SO_4; 2, 2′ – NaCl; 3, 3′ – $CaCl_2$; 4 – H_2O.

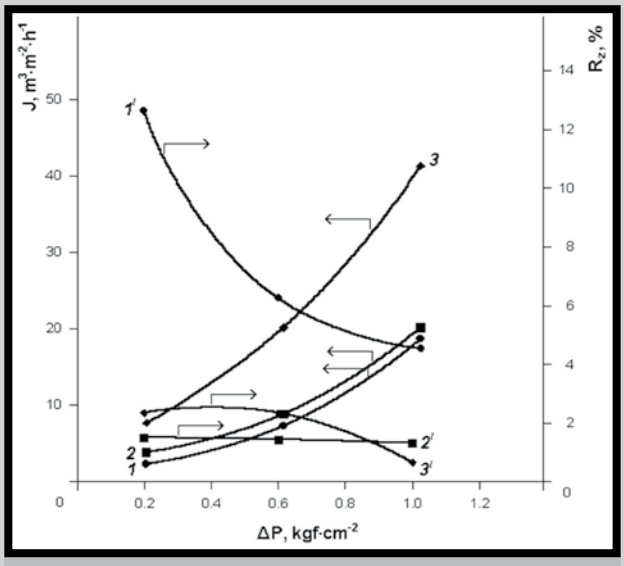

FIG. 4. Dependence of effectiveness by filtrate (J) and inhibitory action (R_z) upon pressure differential (ΔP) at ultrafiltration of salt solutions for hydrogel membranes based on PVA-PVP-HEMA-GMA (δ = 30 μm).
C_{salt} = 0,1 mol/l; 1,1′ – NaCl; 2,2′ – $CaCl_2$; 3, 3′ – Na_2SO_4.

Transport and inhibit mechanisms depend upon hydrogel chemical nature. Thus, effectiveness of hydroxyl-containing hydrogel membrane based on PVA-HEMA at ultrafiltration of sodium sulphate decreases in 2-3 times compared with the transport of calcium and sodium chlorides. Such membrane has a higher inhibitory action for sodium sulphate and less selectivity for chlorides. Moreover, the selectivity is approximately the same for all chlorides, regardless of cation size (FIG. 2). We may assume that in such a case the values of ion charge and ion polarization activity are of great importance. At the same time, at ultrafiltration the effectiveness of both chlorides is practically the same.

Ultrafiltration characteristics of hydrogel membranes with a combined polymeric matrix, when PVP macromolecules containing –NCO group were introduced into a hydroxyl-containing matrix, differ from membranes characteristics based on PVA-HEMA. The effectiveness of membranes based on PVA-PVP-HEMA decreases compared with that of PVA-HEMA membranes. Moreover, the effectiveness is practically the same within the range of pressure differential prior to 1.5 kgf/cm^2 (FIG. 3). On the contrary, the inhibitory action of such membranes considerably increases. With the following increase of pressure differential it decreases from 40 to 20% (FIG. 3). Obviously, it is connected with a gel compacting due to the chains conformational changes under pressure.

The introduction of GMA hydrophobic fragments into the copolymer with the combined polymeric matrix (PVA-PVP-HEMA-GMA) (FIG. 4) determines the essential decrease of effectiveness for both chlorides. Moreover, the effectiveness related to sodium sulphate is the same as that for membranes based on PVA-PVP-HEMA. Selectivity related to sodium chloride at small pressure differential (R_z = 50% at 0.2 kgf/cm^2) slightly increases and inhibitory action by sodium sulphate decreases, especially with the increase of pressure (R_z = 2.5% at 1 kgf/cm^2).

Conclusions

It has been established that nature of polymeric matrix (PVP, PVA or their mixture), which is a structural element of hydrogel and which ensures mechanical properties of the obtained material, is the determinative factor affecting the diffusive characteristics of hydrogel membranes. Macromolecule segments in the internodal space of three-dimensional net possess active functional groups (–OH, –AlkOH, –NCO), which surely affect the diffusion of polar compounds through them.

The obtained results show that diffusive-transport characteristics of investigated hydrogel membranes are defined not only by their water content but by the structure of polymeric matrix (first of all by the chemical structure of polymeric net fragments) as well. This fact offers the challenge for controlled synthesis of biologically compatible hydrogel membranes with high permeability depending upon their practical application.

References

[1] Plate N., Valuyev I. Polymers in contact of live organism. Moscow: Znaniye 1987.
[2] Suberlyak O., Skorokhoda V., Semenyuk N. The of structure and immobilization activity of of PVP of cross-linked copolymers. Engineering of Biomaterials 10, 63-64 (2007) 14-15.
[3] Suberlyak O., Skorokhoda V., Melnyk J. Hydrogel membrane on the basis co(polyvinylpyrrolidone-gr-oxyethylenemethacrylate) in the processes of dialysis. Funkcionalni Materiay 3 (1995) 354-357.
[4] Shvarc A, Grigorovskaya V. At the question about value of link crossing concentration. Colloid Journal 1 (1985) 30-34.
[5] Suberlyak O., Tkhir I., Skorokhoda V. About mechanical properties of polyvinylpyrrolidone graft copolymers. Chimiya, Technolohiya Rechovyn ı Yikh Zastosuvannia (Publishing House of Lviv Polytechnic National University) 260 (1992) 57-59.
[6] Dubyaga V., Perepechkin L., Katalevskiy Ye. Polymeric Membranes. Moscow: Khimiya 1981.
[7] Bryk M., Tsapyuk Ye. Ultrafiltration. Kyiv: Naukova Dumka 1989.
[8] Suberlyak O., Skorokhoda V., Melnyk J. Influence of physical and chemical effects of matrix polymerization polyvinylpyrolidone-(meth)acrylates compositions on diffusive transport descriptions of hydrogel membranes. Chimichni Nauky i Technolohiyi ("Kyiv Mohyla Akademy" Publishing House) 66 (2007) 33-38.
[9] Jones S., Martin G., Royall P., Brown M. Biocompatible polymer blends: effects of physical processing on the molecular interaction of poly(vinyl alcohol) and poly(vinyl pyrrolidone) J. Appl. Polym. Sci. 5, 98 (2005) 2290-2299.
[10] Suberlyak O., Melnyk J., Skorokhoda V. Functionally active polymeric membranes are a respectively type of membranes for the natural processes. Chimichna Promyslovist' Ukrayiny 4 (1999) 42-46.

COATING OF POLY(L-LACTIDE-*CO*-GLYCOLIDE) SCAFFOLDS WITH COLLAGEN/ GLYCOSAMINOGLYCAN MATRICES AND THEIR EFFECTS ON OSTEOBLAST BEHAVIOUR

I. Wojak[1], E. Pamuła[1], P. Dobrzyński[2], H. Zimmermann[3], H. Worch[3], D. Scharnweber[3], V. Hintze[3]*

[1] Department of Biomaterials,
Faculty of Materials Science and Ceramics,
AGH University of Science and Technology, Krakow, Poland
[2] Center of Polymer and Carbon Materials,
Polish Academy of Sciences, Zabrze, Poland
[3] Institute of Materials Science,
Max Bergmann Center of Biomaterials,
Technische Universität, Dresden, Germany
* e-mail: Vera.Hintze@tu-dresden.de

Abstract

Collagen type I and glycosaminoglycans (GAGs) were immobilized on the surfaces of two types of porous biodegradable poly(L-lactide-co-glycolide) (PLGA) scaffolds with pore size in the range of 250-320 μm and 400-600 μm. Two methods of coating were evaluated differing in the way of how the fibrillogenesis solution was introduced into the pores. The distribution of the immunostained collagen in the volume of the scaffolds was analysed with a laser confocal microscope (LSM). The total amount of collagen and GAGs was measured by Sirius Red and Toluidine Blue assays, respectively. The potential of the scaffolds for cell colonization and differentiation was tested in a dynamic cell culture system using human osteosarcoma cells (SAOS-2). The proliferation of SAOS-2 cells was measured by determining the DNA content on days 2 and 7, while differentiation was analyzed by Calcium- and Phosphate-Assays on days 7 and 14. Differentiation of cells was improved by increasing the pore diameter of the scaffolds, and artificial extracellular matrix (aECM) coatings had an additional positive effect for the scaffolds of both pore sizes.

Keywords: *poly(L-lactide-co-glycolide), scaffolds, collagen type I, glycosaminoglycans, hyaluronan, chondroitin sulfate, osteoblasts*

Abbreviations used in the text

aECM	*artificial extracellular matrix*
BSA	*bovine serum albumin*
CS	*chondroitin sulfate*
ECM	*extracellular matrix*
EtO	*ethylene oxide*
GAGs	*glycosaminoglycans*
LSM	*laser confocal microscope*
PBS	*phosphate-buffered saline*
PLGA	*poly(L-lactide-co-glycolide)*
SAOS-2	*osteosarcoma cells*
SEM	*scanning electron microscope*
sHya	*sulfated hyaluronan*

[Engineering of Biomaterials, 86 (2009), 9-13]

Introduction

Resorbable polymers like aliphatic polyesters (polylactides, polyglycolide and co-polymers) have been widely investigated as potential scaffolds for tissue engineering. According to their good biocompatibility, resorbability and attractive mechanical properties these copolymers are promising materials to manufacture products for tissue engineering [1].

However, resorbable polymers without surface modification are not able to elicit required biological response, because they do not have ligands for cell receptors on their surface. Furthermore, they are not able to trigger adsorption of required proteins from serum (e.g. fibronectin, vitronectin, and collagen) in a way similar to other specially designed surfaces, e.g. oxygen-plasma modified polystyrene used to produce tissue culture dishes. For this reason aliphatic polyesters are not optimal for cell adhesion [2].

The biological integration of an implant depends in major part on the interaction between the implant surface and the cells of the host tissue. Hence, many strategies to modify the implants creating optimally suited surface properties for cells have been developed. Some of those methods alter surface topography (e.g., sandblasting, acid etching) or provide a calcium phosphate phase on the surface originally present in bone tissue (hydroxyapatite) [3-5]. Another strategy is the use of organic ECM components in the coating of the implants in order to mimic the natural environment of the cells. Recent studies have shown that ECM serves not only as a scaffold facilitating cell adhesion but also influences cellular function and responses depending on its composition [6]. Coatings utilizing these abilities for improving the biological acceptance of implants should thus enhance not only cell adhesion, but also specific cellular functions which are necessary for the implant integration.

Collagen type I is the major structural protein and constitutes 90% of the protein matrix in adult bone, and has been used successfully as a scaffold for guided bone regeneration [7]. It was found that addition of chondroitin-4-sulfate and dermatan sulfate to collagen type I fibrils improved osteoblast adhesion and differentiation [8]. Titanium alloy pins covered with type I collagen or type I collagen and chondroitin-4-sulfate significantly enhanced bone remodeling in the early stages of bone healing, eventually leading to increased bone formation at the implant surface after 4 weeks *in vivo* [9].

The aim of this study was to improve osteoblasts adhesion and functions on resorbable scaffolds by coating them with artificial matrices consisting of collagen and/or glycosaminoglycans. In this study we used two types of poly(L-lactide-co-glycolide) (PLGA) scaffolds from the same basic material and with the same porosity, but different pore size. The scaffolds were fabricated by solvent/casting and particulate leaching technique.

Materials and methods

Materials

Copolymerization of L-lactide and glycolide was performed in bulk with zirconium acetylacetonate as a biocompatible initiator, according to a method described previously [10]. Briefly, it was performed by ring opening polymerization of L-lactide and glycolide (both from Purac, Netherlands) at 100°C. In order to remove non-reacted monomers, the obtained copolymer was dissolved in chloroform, precipitated with cold methanol and finally dried in vacuum at 50°C to a constant weight.

The copolymer composition was determined by ^{1}H NMR measurements and revealed that the molar ratio of L-lactide to glycolide in the copolymer PLGA was 85:15. Molecular masses were 80 kDa (*Mn*) and 152 kDa (*Mw*), as studied by gel permeation chromatography.

The scaffolds were produced by the modification of a classical solvent casting/particulate leaching technique. Sieved sodium chloride particles (POCh, Gliwice, Poland) of defined size of 250-320 μm or 400-600 μm, were mixed with 10% (w/v) copolymer solution in methlylene chloride (POCh, Gliwice, Poland) in such proportions that a salt volume fraction of 85% was obtained (specifically, 4.707 g NaCl was mixed with 5 ml of 10% w/v polymer solution in methylene chloride). The mixture was transferred into polypropylene vials (diameter 12 mm, 5 ml volume) and air dried overnight, followed by vacuum treatment for 24 hours. Next, the vials with the rigid salt/polymer mixture were cut into slices of the thickness of 2 mm and placed into 100 ml of ultra-high-purity water (UHQ-water, produced by Purelab UHQ-PS apparatus, Elga, U.K.). The water was exchanged several times until the conductivity of the water after washing was ≤ 2 μS/cm. The samples were then dried in a vacuum oven at 35°C for at least 24 h. The preparation procedure is described in detail in ref. [11].

In this study bovine collagen type I (BD Bioscience, Erembodegem, Belgium) and two GAGs were used: 1) sulfated hyaluronan (sHya) with a sulfur content of 6.6% and degree of substitution of 1.0 (INNOVENT e.V., Jena, Germany), 2) chondroitin-4-sulfate (CS) with a sulfur content of 5.1% (Sigma-Aldrich, Schnelldorf, Germany).

Methods for Scaffold Preparation and Characterization

Preparation of fibrillogenesis solution and coating of PLGA scaffolds

First, sHya and CS were dissolved in ice-cold fibrillogenesis buffer (50 mM Na_2HPO_4, 10 mM KH_2PO_4, 270 mM NaCl, pH 7.4) to a concentration of 1 mg/ml and bovine collagen-I was dissolved in ice-cold 10 mM acetic acid to a concentration of 1 mg/ml. Second, the fibrillogenesis solution was prepared by mixing both compounds at a ratio of 1:1 reaching a final collagen concentration of 0.5 mg/ml. The scaffolds were pre-wetted with 70% EtOH and washed in deionized water. Pre-wetted scaffolds were incubated in fibrillogenesis solution according to the following two methods:

Method 1:

10 scaffolds were transferred to a 20 ml syringe. 10 ml of the fibrillogenesis solution was sucked and the syringe was plugged with a latex glove. The piston was pulled until the air bubbles escaped from the scaffolds under low-pressure conditions. The plug was then released to balance the air pressure. The procedure was repeated 10-15 times. The syringes with scaffolds in fibrillogenesis solution were then incubated at 37°C overnight [11].

Method 2:

Scaffolds were transferred to Petri dishes filled with fibrillogenesis solution and placed into a desciccator. Vacuum was applied for 10 min by a rotary pump, and the desciccator was then moved to a 37°C cabinet and collagen fibrillognesis proceeds overnight.

Following, the scaffold were washed 3 times in deionized water, pre-freezed at -80°C for 30 min and subsequently freeze-dried for 3 days. Afterwards, the scaffolds were sterilized with ethylene-oxide and allowed to degas for two weeks.

Scanning electron microscopy (SEM) and determination of porosity

The microstructure of the scaffolds was observed by scanning electron microscopy (SEM, DSM 1982 Gemini, Carl Zeiss, Oberkochen, Germany). Porosity of the scaffolds was calculated from the mass, the dimensions and density of the PGLA, according to the method described previously, and expressed as mean and confidence interval (α = 0.95) [11].

Laser scanning microscopy (LSM) and immunohistochemistry

Collagen type-I was immunostained and its distribution within the scaffolds was analysed using laser scanning microscopy (LSM 510 Meta, Carl Zeiss, Jena, Germany). In brief, immunostaining was performed on a shaker and two controls were prepared: for the first control no antibodies were used, but 1% BSA in PBS, while for the second control no primary, but secondary antibodies were used. Coating on the scaffolds was fixed with 3.7% paraformaldehyde in PBS for 10 min, followed by washing of each scaffold 5 times in 1 ml PBS for 1 min. Unspecific binding was blocked with 1 ml 1% BSA in PBS for 30 min. Scaffolds were incubated with 1 ml of 1:1000 mouse anti-collagen-I (Sigma C2456: primary antibody) in blocking buffer for 60 min. Scaffolds were then washed 5 times for 3 min with blocking solution in PBS. Afterwards, the scaffolds were incubated with 1:200 (10 μg/ml) anti-mouse Alexa Fluor 546 in blocking buffer for 60 min in the dark. After each addition of the antibodies the scaffolds were washed 5 times for 3 min each with blocking solution in PBS. Finally they were stored, protected from light in PBS at 4°C until examined using LSM.

Determination of collagen amount on scaffolds

The collagen concentration immobilised on PLGA scaffolds was quantified using the Sirius Red protein assay. Samples were incubated for 1 h at room temperature in a saturated reagent solution consisting of 500 μl of picric acid with 0.1% Sirius Red, shaking. After washing extensively for eight times with 1 ml washing solution (0.01 M HCl), scaffolds were dried at 37°C overnight. 500 μl measuring solution (0.1 M NaOH) was added and incubated shaking until the scaffolds were decolorized. Absorbance was measured at 540 nm (Tecan Spectrafluor Plus, *Tecan* GmbH, Crailsheim, Germany).

Determination of GAG amount on scaffolds

The GAGs concentration on PLGA scaffolds was quantified using the Toluidine Blue assay. Scaffolds were incubated 4 h at room temperature in 1 ml toluidine solution (0.4 mg/ml toluidine blue in 0.1 M HCl containing 2 mg/ml NaCl), shaking. Scaffolds were washed in deionized water, and incubated for 1 h in 1 ml measuring solution (1 volume 0.1 M NaOH + 4 volumes 100% ethanol), shaking. Absorbance was measured at 530 nm (Tecan Spectrafluor Plus).

Cell culture on PLGA scaffolds

For this experiment the following scaffolds were used: 1) non-coated, 2) coated with collagen type I, 3) coated with collagen type I and sHya, 4) coated with collagen type I and CS. The scaffolds were incubated in McCoy´s medium (15% FBS, 1% Pen/Strep, 2 mM L-glutamine) and placed in the Spinner bottles overnight at 37°C with 5% CO_2. Next day medium was exchanged and 5 million SAOS-2 cells were introduced into each bottle (~500 ml). After 48 h, 7.8 mM β-glycerophosphate and 0.3 mM ascorbic acid were added. SAOS-2 cells were cultivated at 37°C and under a 5% CO_2 atmosphere for 14 days. Scaffolds were harvested after 2, 7, and 14 days in culture, and frozen at -80°C until submitted to further assays.

DNA determination

Scaffolds were defrosted on ice for 30 min. Lysis buffer (1% Triton X-100 in PBS) was added. The scaffolds were incubated in lysis buffer for 50 min on ice, afterwards ultrasound was applied for 10 min and the liquid was additionally mixed with the use of a pipette. Lysate was moved to Eppendorf vials and kept on ice. For fluorescence measurements 10 µl of the lysate was poured in a dark 96-well plate. DNA color solution was prepared by diluting PicroGreen fluorescence dye (Molecular Probes, MoBiTec, Göttingen, Germany) with TE buffer (10 mM TRIS base, 10 mM EDTA, pH 7.5) at a concentration ratio of 1:800. Then 190 µl of DNA color solution was poured into each well and incubated for 10 min at room temperature. Excitation was performed at 485 nm and emission was measured at 535 nm using a Tecan Spectrafluor Plus.

Ca-Assay

For determination of calcium ions the scaffolds were incubated with 0.25 M HCl. A calcium liquicolor (Greiner, H 100 11) kit was used to determine the Ca^{2+} concentration in the scaffolds and was performed as described by the manufacturer. In brief, 10 µl lysate were placed in a 96 well plate and 350 µl dye was added. The samples were measured within 30 min at 590 nm (Tecan Spectrafluor Plus).

Phosphate determination

For determination of phosphate ions scaffolds were incubated with 0.25 M HCl. A phosphate FS kit from DiaSys (Greiner) was used to determine the phosphate concentration in the scaffolds and was performed as described by the manufacturer. In brief, 10 µl of lysate or standard were mixed with 350 µl of dye in a 96 well plate. The samples were measured within 60 min at 340 nm (Tecan Spectrafluor Plus).

Results

The microstructure of the scaffolds obtained by scanning electron microscopy (SEM) is shown in FIG. 1. SEM revealed that the scaffolds of both pore sizes (200-320 µm and 400-600 µm) consist of interconnected, tortuous pores which are oval, circular or irregularly shaped. The diameters of the pores were close to the size of the salt particles used as porogens. Porosity of all samples was 85 ± 1%, e.g. similar to that which had been assumed in the preliminary theoretical design of the scaffolds (salt volume fraction of 85%).

FIG. 2 presents the distribution of collagen within the scaffolds which were infiltrated with fibrillogenesis solution according to two different methods. In method 1 collagen was homogenously distributed on the surface and inside the scaffolds being on the pore walls (FIG. 2 A, B). In method 2 collagen was adsorbed preferentially on the scaffold surface (FIG. 2 C), while inside the scaffolds less collagen was visible (FIG. 2 D). Thus, method 1 seems to be more effective in coating the entire volume of the PGLA scaffolds than method 2.

TABLE 1 presents concentrations of collagen type I and GAGs within the scaffolds determined by Sirius Red and Toluidine Blue assays, respectively. The incubation of the scaffolds in collagen solution led to the immobilization of approximately 170 µg of collagen type I per scaffold. The incubation of the scaffolds in the fibrillogenesis solution containing collagen and sHya or collagen and CS led to the immobilization of approximately 113 µg or 193 µg collagen type I and 150 µg of sHya or 291 µg of CS per scaffold, respectively.

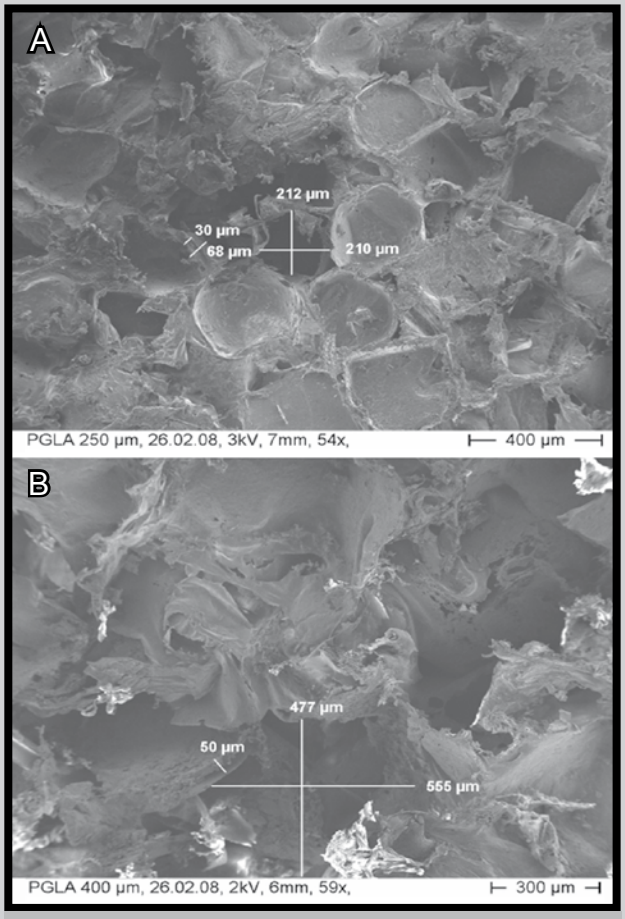

FIG. 1. SEM microphotographs of PGLA scaffolds with pore sizes of 250-320 µm (A) and 400-600 µm (B), respectively.

FIG. 3 presents the number of cells on the scaffolds evaluated by DNA content measurements after 2 days of cultivation. It follows that on the non-coated scaffolds about 200 000 - 300 000 cells were detected. Scaffolds of the pore size of 400-600 µm coated with collagen-I/CS exhibited the tendency of harboring higher number of living cells after 48 h, however results were not statistically different. The analysis of the scaffolds by fluorescence microscopy confirmed the presence of cells on all scaffold surfaces (data not shown). On day 7 the number of cells on all the materials considerably decreased (data not shown).

The calcium and phosphate contents on days 7 and 14 showed that almost all scaffolds (except for non-coated scaffolds with small pores size, e.g. 250-320 µm) presented similar behavior (FIG. 4,5): A significant increase in calcium and phosphate concentrations at 14 days in comparison to 7 days in culture was detected for all surfaces except two samples (e.g. collagen coating and collagen with CS coating on 250-320 µm scaffolds). The blank samples (scaffolds without cells) after 14 days of incubation in culture medium exhibited very low levels of calcium and phosphate.

Discussion

The aim of this study was to: i) develop a method assuring homogenous coating of the aECMs consisting of collagen type I and/or GAGs within the entire porous structure of PLGA scaffolds; ii) characterize the aECM coatings regarding the concentration of the organic components, e.g. collagen type I and/or GAGs; iii) study osteoblast-like cell reaction to unmodified scaffolds and scaffolds coated with aECMs.

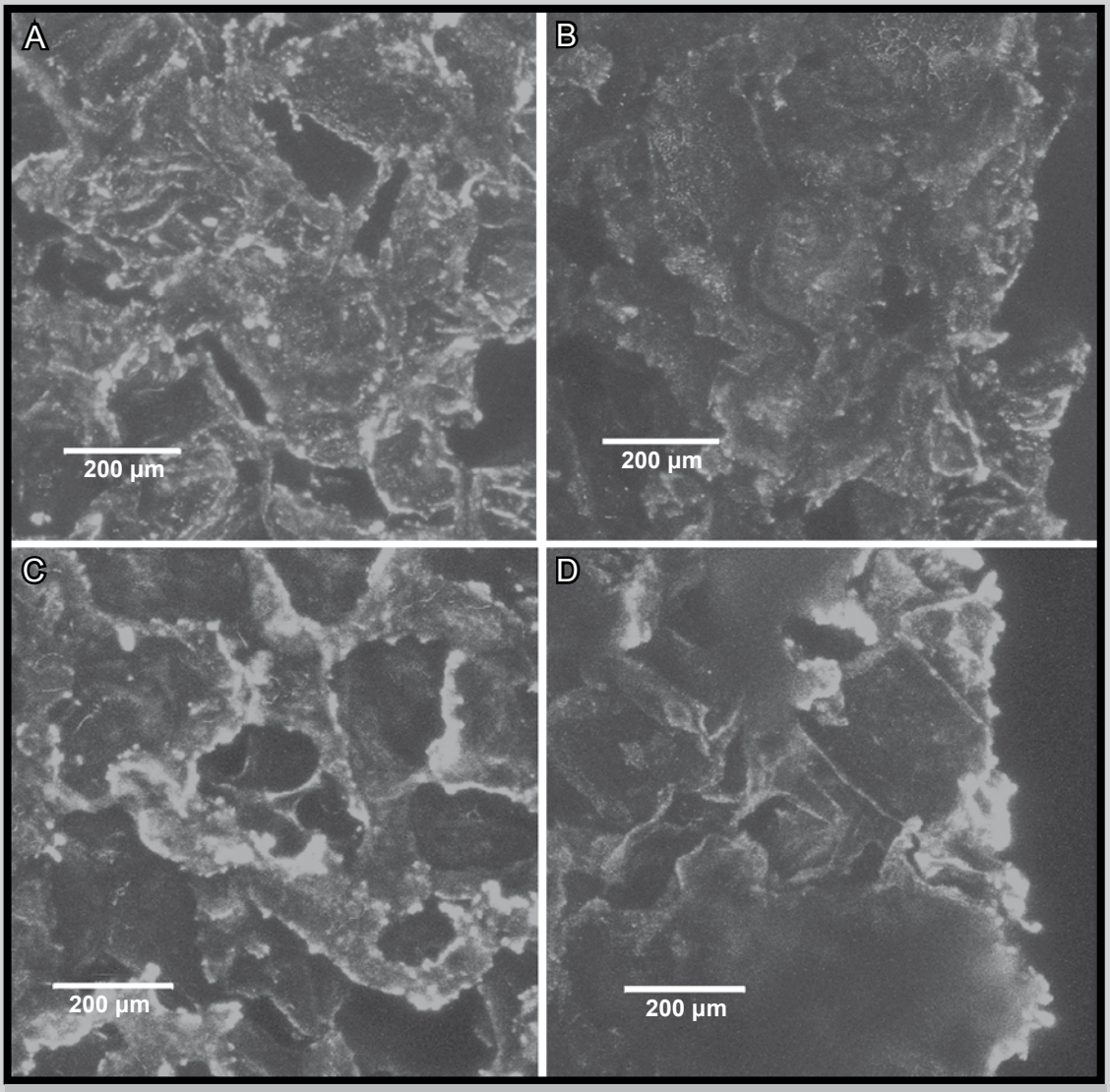

FIG. 2. LSM pictures of PLGA scaffolds of defined pore size 250-320 µm coated with collagen by method 1 (A, B) and method 2 (C, D); top view (A, C) and cross section (B, D). Immunofluorescence staining of collagen in red. Bar 150 µm.

The microstructure of PLGA scaffolds as characterized by SEM showed an open porous structure with defined pore size, similar to that observed in our previous study was proven [12]. The high amount of open porosity as shown in FIG. 1 is a prerequisite for both, homogenous immobilization of aECM and cell seeding on the whole scaffold surface.

PLGA is a hydrophobic material and for this reason it is difficult to force fibrillogenesis solution to enter all pores of the scaffolds. Thus samples pre-wetted by a treatment with 70% EtOH and washed in deionized water were used for immobilization of collagen and GAGs. LSM observation confirmed that applying additionally low-pressure conditions with the syringe (e.g. method 1) is a more effective way to coat the scaffolds homogenously with aECM than a conventional method using a rotary pump (e.g. method 2).

According to Sirius Red and Toulidine Blue assays it was found that incubation of the scaffolds in the fibrillogenesis solutions containing collagen and sHya or CS resulted in immobilization of different amounts of collagen. The quantity of collagen immobilized on PLGA scaffolds was increased when CS was present in the fibrillogenesis solution.

Around 300 000 osteoblast-like SAOS-2 cells could be detected on coated and non-coated scaffold surfaces after two days in culture. However, their number decreased considerably after 7 days in culture. It is probable, that it was caused by residues of sterilization gas (EtO), which was not completely removed during aeration, as previously reported by others [13]. It must be kept in mind that the PLGA scaffolds have very high relative surface area and tortuous pores in which toxic gas molecules could be trapped, and when released may harm the cells. Moreover, ethylene oxide apart from its cytotoxicity and mutagenicity is a very reactive gas, thus chemical reactions between EtO and PLGA and/or GAGs influencing their properties are possible.

TABLE 1. Concentration of collagen and GAGs in PGLA scaffolds of a defined pore size of 250-320 µm coated with collagen type I, collagen I/sHya, and collagen I/CS.

Scaffold	Coating	Collagen amount µg/ scaffold	GAG amount µg/ scaffold
1	Non-coated	n.d.	n.d.
2	Collagen I	170 ± 4	n.d.
3	Collagen I/sHya	113 ± 14	150 ± 8
4	Collagen I/CS	193 ± 5	291 ± 9
n.d. – not detected			

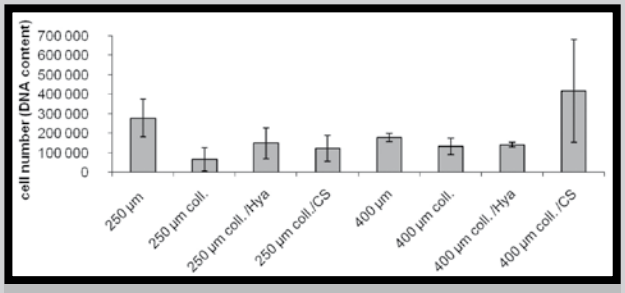

FIG. 3. Number of SAOS-2 cells (by DNA determination) on PLGA scaffolds cultivated for two days. No statistical difference according to t-test.

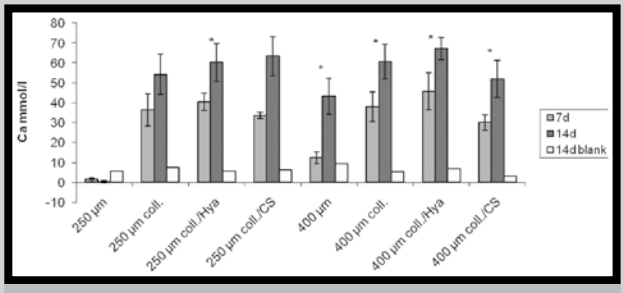

FIG. 4. Concentration of calcium released by SAOS-2 cells on PLGA scaffolds. Asterisks indicate significant difference ($p < 0.05$) compared to 7 days and blank within one group.

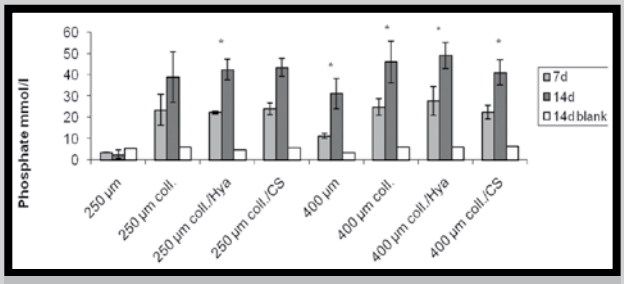

FIG. 5. Concentration of phosphate released by SAOS-2 cells on PLGA scaffolds. Asterisks indicate significant difference ($p < 0.05$) compared to 7 days and blank within one group.

The results of calcium and phosphate contents show that the cells cultivated on the scaffolds with the smaller pore size do not provoke mineralization at day 7 and 14 in cell culture. This suggests that the size of pores is important for the condition of cells, and the osteoblasts prefer larger pores. Similar observations were found in our previous study when osteoblast-like MG63 cells were cultured on the scaffolds with different microstructures: among scaffolds with pore sizes of 180-200 µm, 250-320 µm, and 400-600 µm the largest pores were the most appropriate for cell adhesion, proliferation and differentiation [14]. However, the coating of scaffolds with aECM enhanced matrix mineralization regardless of pore size. The coating with collagen alone was sufficient for this effect, while the addition of GAGs was not significantly improving mineralization. Interestingly, the observed mineralization was not caused by the scaffolds themselves, because the levels of calcium and phosphate were very low on the blank scaffolds (e.g., incubated in culture medium without cells). On the contrary, the observed mineralization was due to osteoblast differentiation.

In conclusion, PLGA scaffolds could be successfully coated with aECMs consisting of collagen and GAGs derivatives. Those coatings make the scaffolds more suitable for bone tissue engineering. Application of EtO sterilization for PLGA scaffolds is rather questionable.

Acknowledgements

The authors would like to acknowledge Dr. T. Hanke for his help in LSM, H. Zimmermann for cell cultures and O. Trommer for SEM evaluation. The financial support of Polish Ministry of Science and Higher Education Grant NN 507280736 and LLP Erasmus Program are also gratefully acknowledged.

References

[1] Vert M., Polymeric biomaterials: Strategies of the past vs. strategies of the future. Prog Polym Sci 32, 2007, 755-761.
[2] Harbers G.M., Grainger D.W., Cell-material interactions: Fundamental design issues for tissue engineering and clinical considerations W Guelcher S. A., J.O. Hollinger (Editors) An introduction to biomaterials, CRC Taylor & Francis, Boca Raton, 2006, 15-45.
[3] Lu X., Leng Y., Zhang X., Xu J., Qin L., Chan C.W., Comparative study of osteoconduction on micromachined and alkali-treated titanium alloy surfaces *in vitro* and *in vivo*. Biomaterials 26, 2005, 1793-1801.
[4] Postiglione L., Di Domenico G., Ramaglia L., di Lauro A.E., Di Meglio F., Montagnani S., Different titanium surfaces modulate the bone phenotype of Saos-2 osteoblast-like cells. Eur J Histochem 48, 2004, 213-222.
[5] Knabe C., Howlett C.R., Klar F., Zreiqat H., The effect of different titanium and hydroxyapatite-coated dental implant surfaces on phenotypic expression of human bone-derived cells. J Biomed Mater Res A 71, 2004, 98-107.
[6] Douglas T., Hempel U., Mietrach C., Heinemann S., Scharnweber D., Worch H., Fibrils of different collagen types containing immobilised proteoglycans (PGs) as coatings: characterisation and influence on osteoblast behaviour. Biomolecular Eng 24, 2007, 455-458.
[7] Rentsch C., Rentsch B., Breier A., Hofmann A., Manthey S., Scharnweber D., Biewener A., Zwipp H, Evaluation of the osteogenic potential and vascularization of 3D poly(3)hydroxybutyrate scaffolds implanted subcutaneously in nude rats. J Biomed Mater Res A (JBMR-A-08-0051), accepted August 2008.
[8] Douglas T., Heinemann S., Mietrach C., Hempel U., Bierbaum S., Scharnweber D., Worch H., Interactions of collagen types I and II with chondroitin sulfates A-C and their effect on osteoblast adhesion. Biomacromolecules 2007, 8, 1085-1092.
[9] Rammelt S., Illert T., Bierbaum S., Scharnweber D., Zwipp H., Schneiders W., Coating of titanium implants with collagen, RGD peptide and chondroitin sulfate. Biomaterials 27, 2006, 5561-5571.
[10] Dobrzynski P., Kasperczyk J., Janeczek H., Bero M., Sythesis of biodegradable copolymers with the use of low toxic zirconium compounds. 1. Copolymerisation of glycolide with L-lactide initatied by Zr(acac). Macromolecules 34, 2001, 5090-5098.
[11] Pamula E., Menaszek E., *In vitro* and *in vivo* degradation of poly(L-lactide-co-glycolide) films and scaffolds. J Mater Sci: Mater Med 19, 2008, 2063-70.
[12] Pamula E., Filova, L. Bacakova, V. Lisa, Adamczyk D., Resorbable polymeric scaffolds for bone tissue engineering: The influence of their microstructure on the growth of human osteoblast-like MG 63 cells. J Biomed Mater Res 89A, 2008, 432-443.
[13] Morejon-Alonso L., Carrodeguas R., Garcia-Menocal J., Perez J., Manent M., Effect of sterilization on the properties of CDHA-OCP-ß-TCP biomaterial. Mater Res 10, 2007, 15-20.
[14] Pamula E., Bacakova L., Filova E., Buczyńska J., Dobrzyński P., Noskowa L., Grausova L., The influence of pore size on colonization of poly(L-lactide-glycolide) scaffolds with human osteoblast-like MG 63 cells *in vitro*. J Mater Sci: Mater Med 19, 2008, 425-435.

3D SIMULATIONS OF DIAMOND MICROFLUIDIC DEVICES

Dariusz Witkowski[1]*, Damian Obidowski[1], Jan Łysko[2]*, Anna Karczemska[1]

[1] Technical University of Lodz,
Institute of Turbomachinery,
ul. Wolczanska 219/223, 90-0924 Lodz, Poland
* e-mail: dariusz.witkowski@p.lodz.pl
[2] The Institute of Electron Technology,
Al. Lotnikow 32/46, 02-668 Warsaw, Poland
* e-mail: jmlysko@ite.waw.pl

Abstract

The aim of this study was to optimize the diamond microfluidic device with four microchannels. The temperature distributions in electrophoretic microchips of different geometries and different materials have been analyzed by the Coventor software. Diamond microfluidic devices are very advantageous over glass or polymer microfluidic devices; they dissipate Joule heat much more efficiently because of the highest thermal conductivity coefficient of diamond.

Keywords: *diamond microfluidic devices, Coventor, Joule heating*

[Engineering of Biomaterials, 86 (2009), 14-16]

Introduction

Diamond reveals several extreme, very beneficial properties - the highest thermal conductivity, remarkable biocompatibility, high electrical breakdown voltage and chemical resistance against the majority of chemical solutions applied in the solid-state technology. This makes diamond thick layers the good choice for the application in microfluidic devices [1-8].

Microfluidic devices are miniaturized systems which transfer tiny quantities of samples and reagents, through a system of microchannels and microchambers made on the surface of a small plate. They are made of different materials; most often of polymers (PDMS, PMMA), glass or silicon.

These systems integrate and reduce a sample size of biochemical reactions and processes. It is a tendency to replace large, often long-lasting and expensive biological and chemical analyses, by microfluidic devices (called sometimes lab-on-a-chip or μ-TAS – micro-total-analysis-systems). A small sample size, low reagent consumption, low waste production and short time of analysis are only a few advantages of these microsystems.

Electrophoresis is a popular method of on-chip separation. It is based on the migration of biomolecules in the electric field. Electrically charged biomolecules (each of different molecular mass or different charge) have different mobilities and the separation can be achieved. In this paper we focus on microfluidic devices based on biomolecule electrophoresis on-chip.

The important issue in designing new microfluidic devices (or electrophoretic chips) is a total analysis of the processes present during the microscale chip electrophoresis. This leads to the optimal selection of the electrophoretic chip material and its optimal geometry [1-3]. The significant and undesirable phenomenon occurring during the process of electrophoresis is Joule heating [1-3,8,9]. This leads to a temperature and gradient growth across the microfluidic channels, decreasing the quality of separation in a number of ways (sample band dispersion or peak broadening, deterioration of analysis resolution and even decomposition of thermally sensitive samples or creation of vapor bubbles in the microchannels). A proper selection of the material with a high thermal conductivity coefficient for chips and optimizing the chip geometry, as well as an efficient cooling system reduce all the above mentioned thermal effects. In our research we focused our interest on different aspects of electrophoretic chips design, with respect to minimizing an influence of Joule heating.

Numerical study

The computer modelling and simulations have been performed with commercial code – CoventorWare™ [11]. The same microchannel geometries were simulated as in the real diamond microfluidic device fabricated in the MNT-ERA NET project DIAMID "Diamond Microfluidic Devices for Genomics and Proteomics" [8]. In this project the diamond microfluidic device was designed for fast electrophoretic separations of DNA and protein molecules.

The geometry was directly introduced into the CoventorWare Process Editor together with the technological steps and material parameters to generate a 3D solid model of the microfluidic device under investigation. Once the 3D model was created, the discretization of the computational domain was performed. The linear "Manhattan Bricks" elements were applied. At this stage, names were assigned to all the faces for the next step - boundary conditions definition.

Calculations were performed for stationary flow conditions. The microfluidic device consists of a plate with the system of four microchannels (FIG. 1), fluid (buffer) inside the microchannels, a support, a cap and air environment. The aim is to optimize the four channel microfluidic device and compare microfluidic devices made of diamond and glass.

The investigations were carried out for a continuous flow at the inlet, for the air flow rate 1000 mm^3/s crosswise the microchannels. The current enforced between the electrodes located at the microchannel terminals was fixed at the common current density value - for the different channel cross-section areas, this common current density assumption gives four different current values: 160, 240, 400 and 800 mA. The air temperature at the inlet, as well as the temperature of the diamond chip bottom wall, were equal to 300K.

KCl 0.1 mol/dm^3 buffer was applied in this model as the liquid inside the channels.

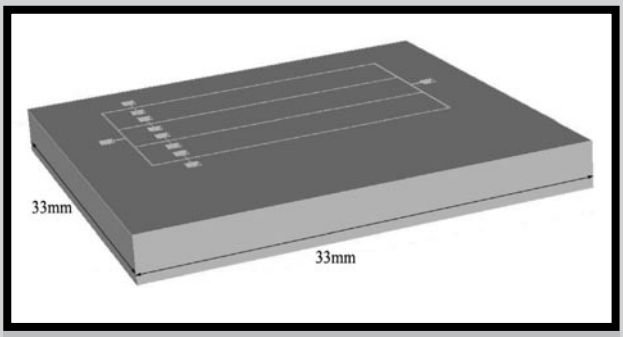

FIG. 1. Model of the chip with the system of microchannels.

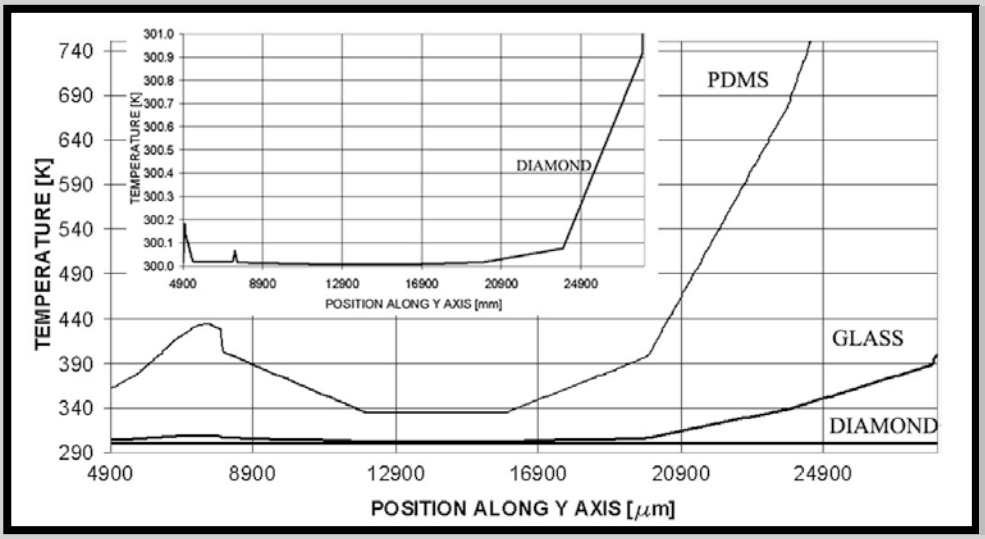

FIG. 2. Temperature profiles along the channels - simulation results for PDMS, glass and diamond chips.

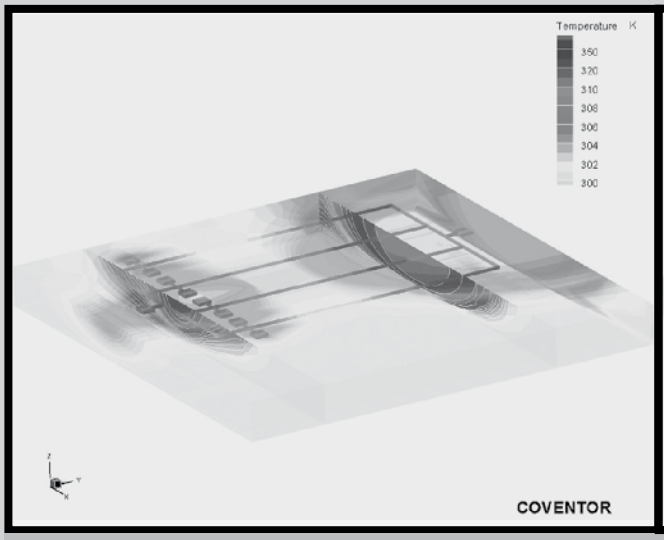

FIG. 3. Glass Microfluidic device & KCl_0,1 mol/dm³ buffer
Channel: depth 250 μm, width 25 μm, length 23200 μm
Current 400 mA, air flow rate 1000 mm³/s along X
Air inlet, TOP & BOTTOM walls temperature fixed 300 K.

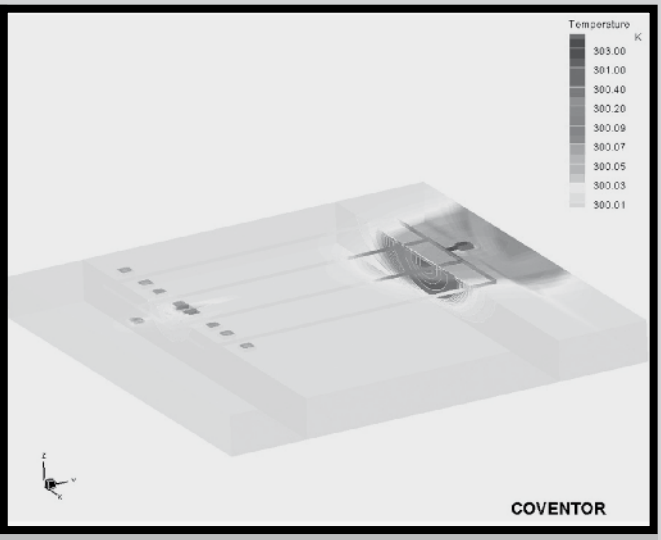

FIG. 4. Diamond microfluidic device & KCl_0,1 mol/dm³ buffer
Channel: depth 250 μm, width 25 μm, length 23200 μm
Current 400 mA, air flow rate 1000 mm³/s along X
Air inlet, TOP & BOTTOM walls temperature fixed 300 K.

Results and discussion

For the first simulations, chips consisting of identical geometry microchannels were applied: depth 250 μm, width 25 μm and length 23200 μm. Different materials were compared: glass, polymer polydimethylosiloxane (PDMS) and diamond. The current enforced between the electrodes was 400mA, the air flow rate was 1000 mm³/s in the perpendicular direction to the microchannel length and the temperature on selected walls was equal to 300K. Significant differences between temperature profiles of the PDMS, glass and diamond chips are well visible. At the channel common inlet of the glass chip, we obtained temperatures exceeding 600K for PDMS and 320K for glass and at the channel outlet terminal even over 350K. The same chip, but made of diamond, reveals a much lower temperature increase, as was expected (FIG. 2).

FIGURES 3 and 4 show the example distributions on diamond and glass microchips with the same microchannels geometries and the same electric field applied. It is clearly seen the difference between both microchips, maximal temperature for diamond microfluidic device is 303K, for glass microfluidic device 350K.

Conclusions

On the basis of the numerical experiment and the analysis performed, it can be stated that diamond is the best material for the application of electrophoretic microchips. In comparison to glass or plastic devices, diamond offers a significant improvement to device performance parameters, it dissipates Joule heat much more efficiently what enables to apply much higher electric field during chip electrophoresis and to obtain much shorter times of separations.

Acknowledgement

Supported by the project „Diamond Microfluidic Devices for Genomics and Proteomics" ERA-NET MNT/98/2006.

References

[1] Witkowski D., Obidowski D., Łysko J., Karczemska A., „3D Simulations of Microfluidic Devices“, Cieplne Maszyny Przepływowe 133 (2008) 359-369.
[2] Karczemska,A., Sideris,D., Hassard,J., Jóźwik,K., Mitura,E., Electrophoretic chips for DNA and protein separations – Joule heating dissipation, VI Sympozjum Modelowanie I pomiary w medycynie MPM, 2004, 9-13 maja 2004, Krynica.
[3] Karczemska,A., Sokołowska,A.: “Materials for DNA sequencing chip”; Journal of Wide Bandgap Materials, Vol. 9, No. 4 April (2002) pp. 243.
[4] Karczemska A., Ralchenko V. Lysko J., Louda P., Kaczorowski W., Hassard J.: Poly-Diamond Device for Microfluid Application, Abstract book of the Vacuum and Plasma Surface Engineering - International Conference, 24th-26th October 2007, Liberec - Hejnice, Czech Republic, pp. 33.
[5] A.Karczemska; “Diamond Microfluidic Devices”, Abstract book of the Vacuum and Plasma Surface Engineering, 26th-27th October 2006, Liberec-Hejnice, Czech Republic.
[6] Björkman, H., Ericson, C., Hjertén, S., Hjort, K.; “Diamond microchips for fast chromatography of proteins”; Sensors & Actuators B 79, 2001, pp. 71-77.
[7] Hassard,J., US Patent 6752914 - Capillary electrophoresis device (2004).
[8] ERA-NET MNT/98/2006, “Diamond Microfluidic Devices for Genomics and Proteomics”, EU project, 2007-2010.
[9] Erickson,D., 2005, Towards numerical prototyping of labs-on-chip: modelling for integrated microfluidic devices, Review, Microfluid Nanofluid (2005) 1: 301-318.
[10] Tang,G., Yan,D., Yang,Ch.,Gong,H., Chai,Ch.,Lam,Y., Joule heating and its effects on electrokinetic transport of solutes in rectangular microchannels, Sensors and Actuators A 139 (2007) pp. 221-232.
[11] Coventor inc. “Microfluidics Reference”, 2008.

WPŁYW ATMOSFERY WYPALANIA NA ZAGĘSZCZANIE, MORFOLOGIĘ I WŁAŚCIWOŚCI SPRĘŻYSTE SPIEKÓW Z NATURALNEGO HYDROKSYAPATYTU

Jadwiga Brzezińska-Miecznik*, Beata Macherzyńska, Krzysztof Haberko, Włodzimierz Mozgawa, Mirosław Bućko, Anna Pyda

Akademia Górniczo-Hutnicza,
Wydział Inżynierii Materiałowej i Ceramiki,
30-059 Kraków, al. Mickiewicza 30
* e-mail: j.brzez@wp.pl

Streszczenie

Naturalny hydroksyapatyt został wyekstrahowany z korowej części długich kości wieprzowych poprzez potraktowanie ich gorącym roztworem NaOH, przemycie H_2O i wyprażenie w temperaturze 450°C. Pod ciśnieniem 200 MPa wyprasowano próbki, które spiekano w atmosferze powietrza, CO_2 i argonu w temperaturze 1000°C. Stwierdzono, że atmosfera spiekania wpływa na zagęszczenie, morfologię, stabilność chemiczną i w konsekwencji na właściwości sprężyste spieków. W wyniku spiekania hydroksyapatytu w powietrzu uzyskano gęste spieki o dużych, wykształconych ziarnach. Próbki spiekane w argonie i w CO_2 charakteryzują się mniejszym zagęszczeniem i drobnoziarnistą mikrostrukturą. Stwierdzono także, że atmosfera CO_2 nie tylko przeciwdziała rozkładowi hydroksyapatytu (nie pojawia się wolne CaO), lecz powoduje wbudowywanie się grup CO_3^{2-} w strukturę.

Słowa kluczowe: *hydroksyapatyt, spiekanie, mikrostruktura, właściwości sprężyste*

[Inżynieria Biomateriałów, 86, (2009), 17-21]

Wprowadzenie

Ceramika hydroksyapatytowa ze względu na swoje podobieństwo chemiczne i mineralogiczne do nieorganicznych składników kości i zębów może być stosowana do wypełniania ubytków zarówno w stomatologii, jak i chirurgii kostnej. Po zaimplantowaniu nie wykazuje bowiem żadnych efektów cytotoksycznych ani kancerogennych. Odznacza się natomiast dużą biozgodnością i bioaktywnością zarówno w stosunku do tkanek twardych, jak i miękkich [1,2].

Istnieją dwa główne rodzaje hydroksyapatytu: naturalny otrzymywany z kości zwierzęcych i syntetyczny otrzymywany na drodze reakcji chemicznych. Obydwa rodzaje hydroksyapatytu mają zastosowanie jako biomateriały. Podstawową różnicą obu rodzajów hydroksyapatytu jest to, że materiał otrzymywany z kości zwierzęcych zawiera w sposób naturalny w swej strukturze grupy węglanowe, magnez, sód, potas oraz inne pierwiastki śladowe, co sprawia, że jego skład chemiczny jest bliższy składowi kości [3].

EFFECT OF SINTERING ATMOSPHERE ON DENSIFICATION, MORPHOLOGY AND ELASTIC PROPERTIES OF NATURAL ORIGIN HYDROXYAPATITE

Jadwiga Brzezińska-Miecznik*, Beata Macherzyńska, Krzysztof Haberko, Włodzimierz Mozgawa, Mirosław Bućko, Anna Pyda

AGH University of Science and Technology,
Faculty of Materials Science and Ceramics,
30 Mickiewicza Av., 30-059 Cracow, Poland
* e-mail: j.brzez@wp.pl

Abstract

Natural hydroxyapatite was extracted from cortical part of long pig bones by treatment in hot sodium hydroxide solution. Material was washed with water, dried and calcined at 450°C. Cylindrical samples compacted under 200 MPa were sintered in air, CO_2 and Ar atmospheres at 1000°C. Sintering atmosphere influences densification, microstructure, chemical stability and consequently elastic properties of the samples. Treatment in air atmosphere leads to the most dense material of the largest and faceted grains. Lower densification and smaller grains occur in CO_2 and Ar atmospheres. Carbon dioxide atmosphere counteracts decomposition of the material, no free CaO appears, but additional CO_3^{-2} groups become built into the HAp structure.

Keywords: *hydroxyapatite, sintering, microstructure, elastic properties*

[Engineering of Biomaterials, 86 (2009), 17-21]

Introduction

Materials based on hydroxyapatite (HAp) are used in dentistry and bone surgery as a filling medium. This is due to the similarity of this material to the mineral part of bones and teeth. No cytotoxic and cancerogenic effects after implantation of this material occur. Hydroxyapatite shows bioaffinity and bioactivity towards both hard and soft tissues [1,2].

Two kinds of hydroxyapatite are applied as biomaterials: synthetic one and extracted from animal bones. The basic feature of the natural origin HAp is presence in its structure of carbonate groups, magnesium, sodium, potassium and other trace elements, usually occurring in living bones [3].

Materials and methods

The starting material was extracted from the cortical part of pig bones from which joint heads were cut off. After boiling in water and removing soft tissues the material was subjected to the treatment in a Teflon vessel at 90°C in 4M NaOH solution for 24 h. Then the material was washed many times with water in order to remove sodium ions until pH=7.5 in the filtrate was achieved. After drying at 120°C and sieving the powder was heat treated in flowing oxygen atmosphere at 450°C for 1 h. This operation allowed us to burn out traces of organic matter remaining in the material.

Materiały i metody

Materiałem wyjściowym, z którego uzyskano hydroksyapatyt, była część korowa wieprzowych kości długich, po uprzednim obcięciu główek. Proces ekstrakcji hydroksyapatytu przebiegał następująco: po częściowym usunięciu szpiku kości gotowano w wodzie, a następnie usunięto tkanki miękkie i część gąbczastą. Dalsze usunięcie substancji organicznej odbywało się poprzez dwukrotne potraktowanie kości 4 M roztworem NaOH w temperaturze 90°C. Czas działania zasady wynosił każdorazowo 24 godziny, a operacja ta odbywała się w naczyniach teflonowych (politetrafluoroetylen). Kolejną czynnością było przemywanie w znacznym stopniu odbiałczanej masy kostnej wodą destylowaną w celu odmycia jonów sodowych. Operację przemywania powtarzano wielokrotnie, aż do uzyskania pH w filtracie równego 7,5. Następnie materiał wysuszono w temperaturze 120°C, rozdrobniono i przesiano przez sito perlonowe. Resztę substancji organicznej starano się usunąć poprzez wstępne prażenie proszku w temperaturze 450°C przez 1 godzinę w atmosferze tlenu.

Wyprażony proszek zmielono w młynie mieszadłowym w środowisku propanolu. Na 150 g proszku zastosowano 1500 g mielników w kształcie kulek o średnicy 2 mm wykonanych z dwutlenku cyrkonu.

Prasowanie proszku odbywało się na sucho, wstępnie jednoosiowo pod ciśnieniem 11 MPa, po czym doprasowano je izostatycznie pod ciśnieniem 200 MPa.

Spiekanie próbek (wyprasek) przeprowadzono w piecu rurowym w temperaturze 1000°C w atmosferze powietrza, argonu i dwutlenku węgla. Postęp temperatury wynosił 5°C/min, czas przetrzymywania w temperaturze maksymalnej wynosił 60 minut, a prędkość przepływu gazu 1 dcm^3/min.

Skład fazowy proszków oznaczono metodą analizy dyfrakcyjnej promieniowania rentgenowskiego bazując na danych zawartych w kartotece ICDD. Wielkość parametrów sieciowych służących do wyznaczenia objętości komórek elementarnych określono metodą Rietvelda.

Wykonano również widma w podczerwieni dla próbek z początkowego i końcowego etapu spiekania (spektrometr Bio-Rad FTS 60 MV). Pomiary przeprowadzono techniką transmisyjną, wykonując pastylki z bromku potasu (homogenizowano 2 mg hydroksyapatytu z 300 mg KBr, następnie prasowano w matrycy 13 mm z odpowietrzaniem pod naciskiem 10 t). Widma rejestrowano w skali absorbancji w zakresie 4000-400 cm^{-1} (MIR), rejestrując 256 skanów ze zdolnością rozdzielczą 4 cm^{-1}. Przypisanie pasm absorpcyjnych przeprowadzono w oparciu o pracę [4].

Gęstość pozorną, porowatość otwartą spieków oznaczono metodą ważenia hydrostatycznego w wodzie. Powierzchnię właściwą przed i po spiekanych próbek oznaczono metodą BET adsorpcji azotu w temperaturze ciekłego azotu stosując urządzenie Quantachrome model Nova 1200e.

Rozkład wielkości porów w wypraskach i po spiekaniu oznaczono metodą porozymetrii rtęciowej stosując urządzenie Quantachrome model PoreMaster.

Obserwacje przełamów spiekanych próbek przeprowadzono wykorzystując skaningową mikroskopię elektronową (Nova Nano-SEM-200). Badania wykonano w Laboratorium Mikroskopii Skaningowej i Mikroanalizy WIMiC, AGH.

Badania właściwości sprężystych wykonano nieniszczącą metodą ultradźwiękową stosując defektoskop ultradźwiękowy UZP-1 (INCO-VERITAS) z dokładności pomiarów czasów przejścia fali ultradźwiękowej ± 0,01 μs.

W badaniach zastosowano metodę przejścia posługując się głowicami ultradźwiękową do fal podłużnych f = 2 MHz, a do fal poprzecznych f = 4 MHz. Jako ośrodek sprzęgający głowicę z badaną powierzchnią płyty stosowano olej parafinowy.

The resulting powder was then attrition ground with 2 mm zirconia balls (TOSOH) in propanol. For 150 g of the powder 1500 g of the grinding media were used.

Uniaxial pressing under 11 MPa and subsequent isostatic pressing under 200 MPa allowed us to manufacture cylindrical samples. Sintering was performed in a tube furnace at 1000°C with 5°C/min rate of temperature increase, in air, argon or carbon dioxide atmospheres with 60 min soaking time.

By the X-ray diffraction phase composition of the samples and volume of the HAp unit cell basing on the ICDD data and using the Rietveld method were determined.

The powder samples (2 mg) were mixed with 300 mg KBr and pressed in order to obtain the IR transmission spectra of the starting and sintered samples, using the Bio-Red FTS 60 MV apparatus. The spectra were recorded in the 4000-400cm^{-1} range with the resolution of 4 cm^{-1}. Identification of the absorption bands was based on the data collected in [4].

Apparent density and open porosity were determined by the hydrostatic weighing. Specific surface area of the powder was determined by the nitrogen adsorption (BET) using the Quantochrome Nova 1200e equipment. PoreMaster (Quantachrome) allowed us to measure the pore size distribution in green and sintered samples. Fracture surface of the sintered samples was investigated under SEM (Nova Nano-SEM-200). Elastic properties were determined by ultrasonic method using longitudinal (f = 2 KMHz) and transverse waves (f = 4 MHz). Equipment applied was UZP-1 (INCO-VERITAS).

Results and discussion

X-ray diffraction (FIG. 1) reveals hydroxyapatite as the only phase in the material sintered in CO_2 atmosphere. However, samples heat treated in air show additionally 1.2% $CaCO_3$ and that in argon - 1.4% CaO. It cannot be excluded that calcium carbonate results from the reaction of CaO with CO_2 present in the ambient atmosphere.

Infrared spectroscopy (FIG. 2) shows that sintering atmosphere influences intensity of the absorption bands which belong to the carbonate groups (1400-1550 cm^{-1} and about 880 cm^{-1}) and from OH^- groups (about 633 cm^{-1} and about 3572 cm^{-1}). Air sintered sample shows decreased integral intensity of the bands 1413 cm^{-1} and 1458 cm^{-1}. In the case of the sample heat treated in Ar intensity of both bands increases, however it concerns more the 1457 cm^{-1} band. Changes of the bands intensities can be attributed to the variation of the CO_3^{-2} groups content in the HAp structure. The remaining IR bands, about 1092 cm^{-1} and 1033 cm^{-1} originate from doubly degenerated asymmetric stretching vibrations v_3 P-O and symmetric stretching vibrations of v_1 P-O correspond to 960 cm^{-1}. Absorption maxima at 600 cm^{-1} and 570 cm^{-1} can be attributed to the triply degenerated bending vibrations v_4 O-P-O. No essential changes of the band at 880 cm^{-1} occur in both spectra. Different behaviour is observed in the sample sintered in CO_2 atmosphere; essential increase of the 1415 cm^{-1}, 1550 cm^{-1} and 880 cm^{-1} absorption bands occur. It was shown in publication [5] that this effect can be attributed to the incorporation of the additional CO_3^{-2} groups to the HAp structure. Most probably these groups occupy the OH^- positions. This seems to be corroborated by the decreased intensity of the absorption bands of hydroxyl groups. Indeed, in the samples sintered in CO_2 atmospheres absorption bands 3572 cm^{-1} and 633 cm^{-1} nearly disappear. Another fact which confirms this conclusion is given by the essentially higher unit cell volume of the samples sintered in CO_2 atmosphere compared to those heat treated in Ar and air atmospheres (TABLE 1).

Wyniki i dyskusja

Rentgenowska analiza fazowa (RYS. 1) wykazała, iż w przypadku próbek spiekanych w atmosferze CO_2 hydroksyapatyt jest jedyną fazą. Natomiast w próbach spiekanych w atmosferze powietrza pojawiło się 1,2% kalcytu, a w próbce spiekanej w atmosferze argonu 1,4% CaO. Prawdopodobnie kalcyt pojawił się w wyniku przejścia w wilgotnym powietrzu CaO do $Ca(OH)_2$ i następnej reakcji z CO_2 z powietrza.

Badania metodą spektroskopii w podczerwieni (RYS. 2) pozwoliły stwierdzić, iż w zależności od atmosfery spiekania zmienia się w stosunku do próbki wyjściowej (niespiekanej) intensywność pasm pochodzących od grup CO_3^{2-} tj. pasm w zakresie liczb falowych 1400-1550 cm^{-1} i ok. 880 cm^{-1} oraz od grup OH^- pasma w przy ok. 633 cm^{-1} i ok. 3572 cm^{-1}. Dla widma próbki spiekanej w atmosferze powietrza zmniejsza się intensywność integralna pasm 1413 cm^{-1} i 1458 cm^{-1}. Dla widma próbki spiekanej w atmosferze argonu intensywność łączna obu pasm zwiększa się, przy czym w większym stopniu dotyczy to pasma przy 1457 cm^{-1}. Zmiana intensywności pasm może być związana ze zmianą zawartości grup CO_3^{2-} w strukturze, a także ze zmianą symetrii tych grup.

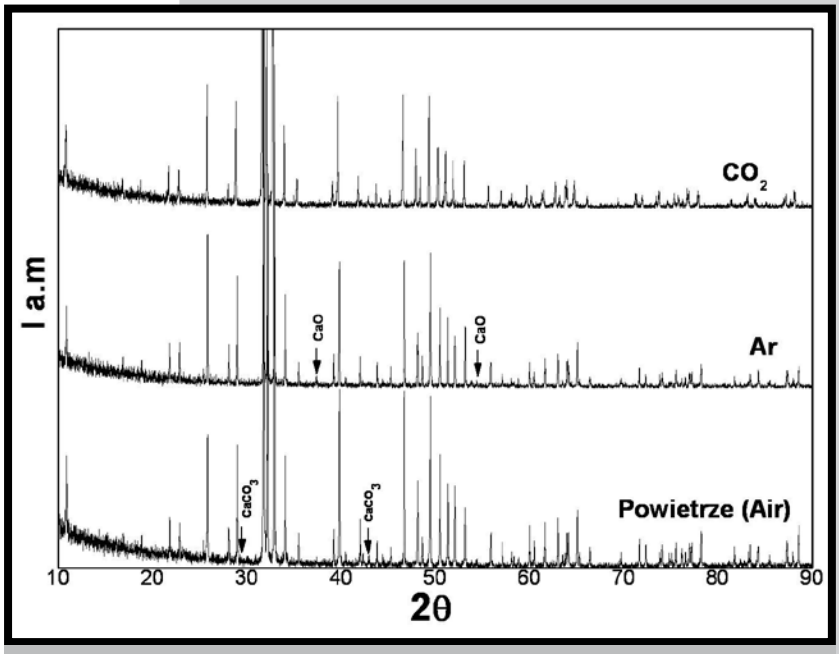

RYS. 1. Dyfraktogramy rentgenowskie próbek spiekanych w różnych temperaturach.
FIG. 1. X-ray diffraction patterns of the samples sintered in indicated atmospheres.

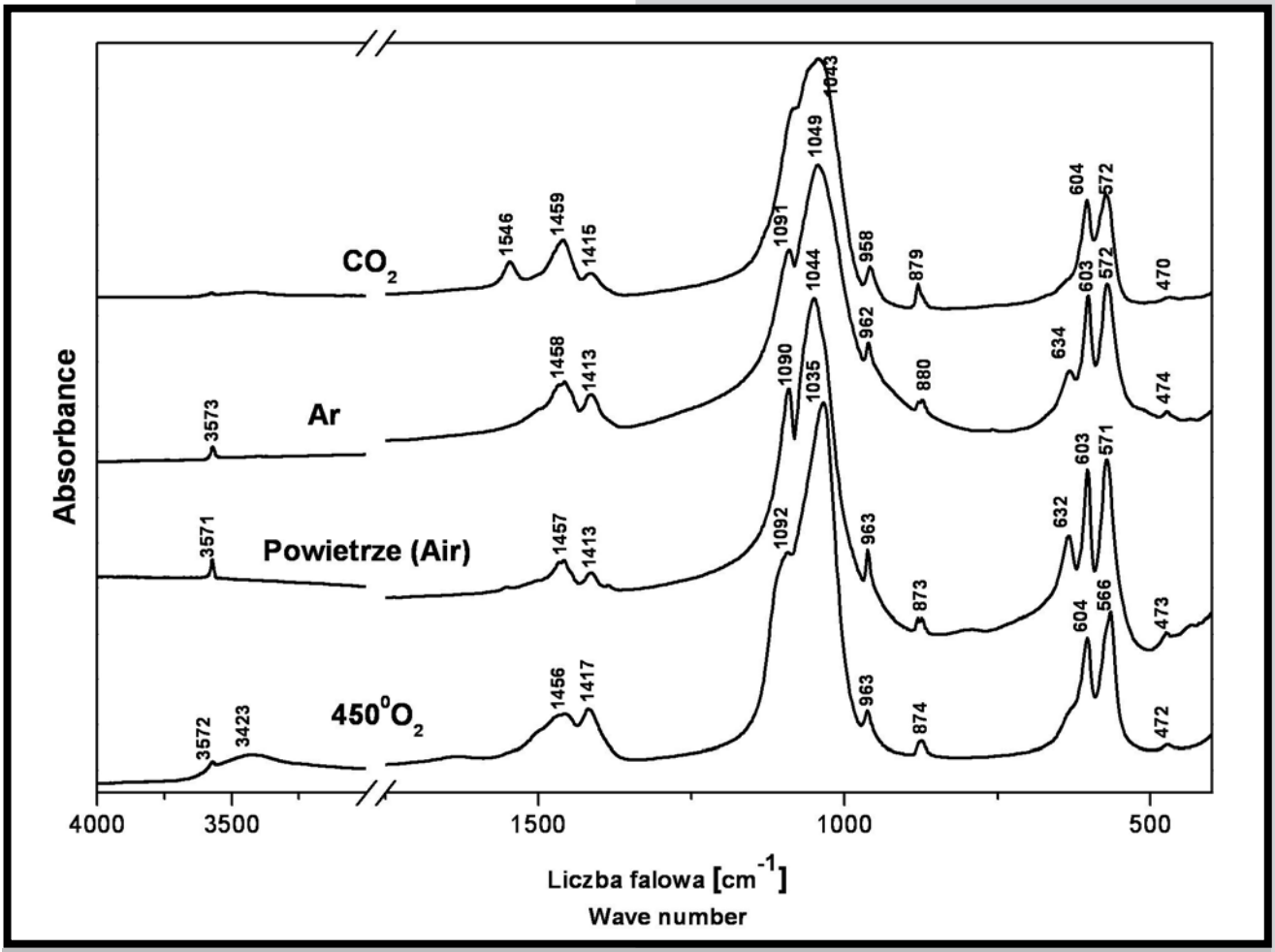

RYS. 2. Widma absorpcyjne w podczerwieni próbek spiekanych w powietrzu, CO_2 i Ar.
FIG. 2. IR spectra of the samples sintered in indicated atmospheres.

TABELA 1. Charakterystyka próbek hydroksyapatytu spiekanych w powietrzu, CO_2 i Ar.
TABLE 1. Characterization of samples sintered in air, CO_2 and Ar.

Atmosfera Atmosphere	Gęstość pozorna Apparent density [g/cm³]	Porowatość otwarta Open porosity [%]	Nasiąkliwość Waterabsobability [%]	Powierzchnia właściwa Specific surface area [m²/g]	Objętość komórki elementarnej Unit cell volume [Å³]
Powietrze / Air	3.08 ± 0.02	0	0	-	528.7
Ar	2.44 ± 0.01	22.06 ± 0.47	8.92 ± 0.40	2.72	528.4
CO_2	2.38 ± 0.03	23.58 ± 0.46	9.91 ± 0.26	2.14	533.4
Wypraska Green samples	1.61 ± 0.03	-	-	79.62 ± 0.5	-

Pozostałe pasma o maksimach absorpcyjnych ok. 1092 cm^{-1} oraz 1033 cm^{-1} pochodzą od potrójnie zdegenerowanych antysymetrycznych drgań rozciągających v_3 P−O. Pasmo przy ok. 960 cm^{-1} pochodzi od symetrycznych drgań rozciągających v_1 P−O. Maksima absorpcyjne przy ok. 600 cm^{-1} i 570 cm^{-1} pochodzą od potrójnie zdegenerowanych drgań zginających v_4 O−P−O. W przypadku pasma ok. 880 cm^{-1} w obydwóch widmach brak istotnych zmian. Odmiennie wygląda sytuacja dla próbek spiekanych w atmosferze CO_2. Na widmach tych próbek widoczny jest bardzo wyraźny wzrost intensywności pasm zarówno 1415 cm^{-1}-1550 cm^{-1} jak i pasma ok. 880 cm^{-1}. Jak wykazano w pracy [5] zjawisko to wynika z wbudowywania się grup CO_3^{2-} w strukturę hydroksyapatytu. Grupy węglanowe wbudowują się prawdopodobnie w pozycję grup OH^-. Potwierdzeniem tego faktu jest zanik pasm pochodzących od grup OH^- w próbkach wypalanych w atmosferze CO_2 (praktyczny zanik pasm przy 3572 cm^{-1} i 633 cm^{-1}). Wskazuje na to również objętość komórki elementarnej, która jest zdecydowanie większa dla próbek spiekanych w atmosferze CO_2 (533,4 Å³) niż dla próbek wypalanych w atmosferze powietrza (528,7 Å³) czy też argonu (528,4 Å³) (TABELA 1).

Zbadano również wpływ atmosfery wypalania na zagęszczenie i morfologię spieków. Wypalaniu poddano wypraski o gęstości pozornej 1,61 g/cm³ (TABELA 1). Rozkład wielkości porów w próbkach był jednomodalny (RYS. 3). Charakterystyka spiekanych próbek została przedstawiona w TABELI 1 i na RYS. 3.

W wyniku spiekania próbek w temperaturze 1000°C w powietrzu uzyskano stosunkowo gęste spieki pozbawione porowatości otwartej. Próbki charakteryzowały się dużymi (rozrośniętymi) ziarnami o dobrze wykształconych ścianach (RYS. 4a). Również gęste spieki, ale o nieco drobniejszej mikrostrukturze otrzymano przez wypalanie próbek w powietrzu w temperaturze 900°C (RYS. 4d). Natomiast próbki wypalane w atmosferze CO_2 lub argonu wykazują znaczną porowatość otwartą, odpowiednio 23,6% i 22,1%, co znajduje odzwierciedlanie w objętości porów (RYS. 3).

W przeciwieństwie do próbek wypalanych w atmosferze powietrza próbki wypalane w atmosferze dwutlenku węgla i argonu zachowują drobnoziarnistą mikrostrukturę. Świadczą o tym również wyniki badań powierzchni właściwej spieków. Wielkość cząstki d_{BET} dla próbek spiekanych w CO_2 wynosi 1,18 µm a dla próbek spiekanych w argonie 0,904 µm.

Również wyniki badań właściwości sprężystych potwierdzają powyższą zależność. Dla spieków otrzymywanych w atmosferze powietrza stałe materiałowe, takie jak moduł Younga i moduł sztywności, są dwukrotnie wyższe od tych wyznaczonych dla próbek spiekanych w CO_2 czy argonie. Dane zawarte w TABELI 2 pokazują, że wraz ze zmniejszeniem się porowatości zwiększają się wartości modułu Younga i modułu sztywności. Dla próbek wypalanych w atmosferze CO_2 i argonu wartości E i G są zbliżone. Z przeprowadzonych badań ultradźwiękowych wynika, że wartość współczynnika Poissona jest taka sama dla wszystkich próbek.

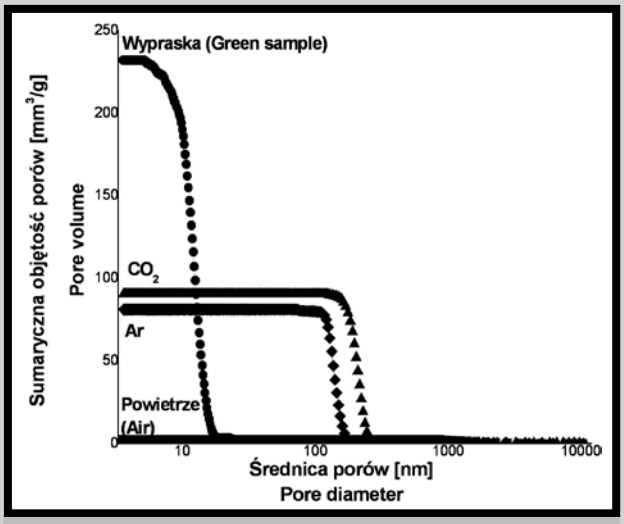

RYS. 3. Rozkład wielkości porów w spiekanych próbkach w zależności od atmosfery wypalania.
FIG. 3. Pore size distribution curves in green and samples sintered in indicated atmospheres.

In TABLE 1 specific surface area, apparent porosity, water absorption and open porosity are given. FIG. 3 shows pore size distribution curves of green and sintered samples. All of them show mono-modal pore size distribution. No open porosity occurs in the samples heat treated in air. SEM observations reveal dense microstructure with relatively big and faceted grains (FIG. 4a). Also dense microstructure in the air sintered at 900°C sample but with smaller grains is shown in FIG. 4d. Densification of samples treated at 1000°C in Ar and CO_2 atmospheres is much lower (TABLE 1). These samples even show open porosity. In both cases, sizes of grains are essentially smaller. As it should be expected Young modulus and modulus of shear strongly depend on the system porosity and hence on sintering atmosphere. Data gathered in TABLE 2 demonstrate the highest Young modulus and shear modulus of the samples treated in air. No effect of the heat treatment atmosphere on the Poisson ratio was noticed.

TABELA 2. Właściwości sprężyste próbek wypalanych w różnych atmosferach.
TABLE 2. Elastic properties of the samples sintered in different atmospheres.

Atmosfera wypalania Sintering atmosphere	Moduł Younga Young modulus [GPa]	Moduł sztywności Shear modulus [GPa]	Współczynnik Poissona Poisson ratio
Powietrze / Air	112.97 ± 1.31	44.24 ± 0.38	0.28 ± 0.01
Ar	48.22 ± 1.52	18.80 ± 0.77	
CO_2	43.10 ± 3.48	16.84 ± 1.35	
Wypraska Green samples	8.47 ± 1.18	3.33 ± 0.39	

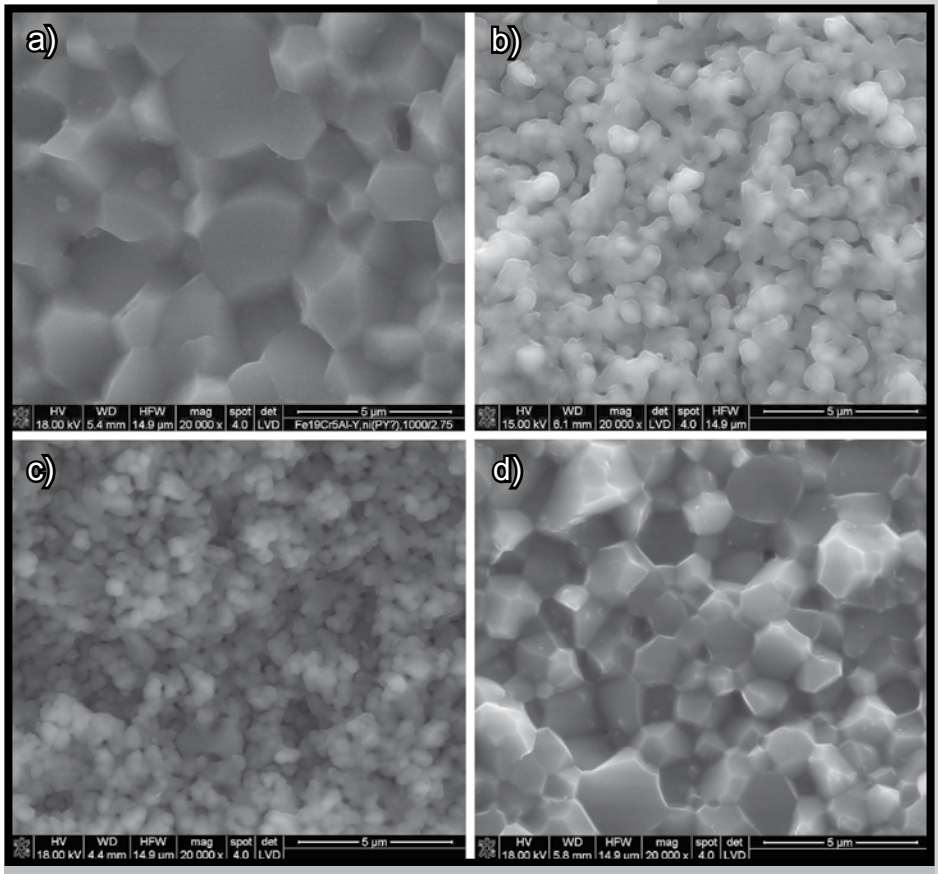

RYS. 4. Mikrofotografie przełamów próbek spiekanych w temperaturze 1000°C w atmosferze: a) powietrza; b) CO_2 i c) argonu; oraz d) próbki spiekanej w temperaturze 900°C w atmosferze powietrza.
FIG. 4. Fracture surfaces of the samples sintered at 1000°C in different atmospheres, a) air, b) CO_2, c) Ar, d) sample sintered in air atmosphere at 900°C for 1h.

Wnioski

Atmosfera wypalania wpływa na stabilność chemiczną hydroksyapatytu, morfologię, stopień zagęszczenia spieków i właściwości sprężyste.

W próbkach spiekanych w 1000°C w atmosferze CO_2 jedyną fazą jest hydroksyapatyt, natomiast w próbkach spiekanych w atmosferze powietrza i argonu pojawia się dodatkowo niewielka ilość wolnego CaO.

Atmosfera CO_2 przeciwdziała zjawisku rozkładu hydroksyapatytu i ponadto sprawia, że następuje wbudowywanie się w strukturę grup węglanowych, najprawdopodobniej w pozycję grup OH^-.

Próbki spiekane w powietrzu charakteryzują się wysokim stopniem zagęszczenia i brakiem porowatości otwartej. Natomiast próbki spiekane w argonie i w CO_2, wykazują mniejsze zagęszczenie i zachowują znaczną porowatość otwartą.

Próbki spiekane w powietrzu charakteryzują się dużymi ziarnami o dobrze wykształconych ścianach, natomiast w próbkach spiekanych w argonie i w CO_2 ziarna pozostają drobne.

Wraz ze zmniejszaniem się porowatości próbki wykazują wyższe wartości modułów Younga i sztywności.

Podziękowanie

Praca finansowana w ramach 6PR projekt NANOKER NR NMP3-CT-2005-515784 oraz SPB nr 139/6. PR UE/2005/7.

Conclusions

1. Atmosphere of the heat treatment affects chemical stability, morphology, density and elastic properties of natural origin hydroxyapatite.

2. Samples sintered in CO_2 atmosphere retain hydroxyapatite structure, but in those sintered in air and argon small fraction of $CaCO_3$ or CaO appear, respectively.

3. Concentration of CO_3^{-2} groups increases in the material sintered in the CO_2 atmosphere. They most probably are substituted for hydroxyl groups.

4. Sintering in air results in dense samples lacking of open porosity. They show relatively big and faceted grains. High open porosity and grains of small sizes occur in samples treated in air or Ar atmosphere.

5. Dense samples show essentially higher Young modulus and shear modulus compared to those poorly densified.

Acknowledgements

This work was supported by 6PR project NANOKER Nº NMP3-CT-2005-515784 and SPB Nº 139/6. PR UE/2005/7.

Piśmiennictwo References

[1] Hench L.L.: "Bioceramics: from concept to clinic", Journal of American Ceramic Society, 74 (1991) 1487-1510.
[2] Chamg B.S., Lee C.K., Hong K.S., Youn H.J., Ryun H.S., Chung S.S.: "Osteoconduction at porous hydroxyapatite with various pore configuration", Biomaterials, 21 (2000) 1291-1298.
[3] Haberko K., Bućko M.M., Brzezińska-Miecznik J., Haberko M., Mozgawa W., Panz T., Pyda A., Zarębski J.: „Natural hydroxyapatite - its behaviour during heat treatment", Journal of the European Ceramic Society, 26 (2006) 537-542.
[4] Farmer C.: The Infrared Spectra of Minerals, Mineralogical Society Monograph 4. Mineralogical Society 41 Quin's, London 1974.
[5] Haberko K., Bućko M.M., Haberko M. Mozgawa W., Carpentier J., Pyda A.: "Transormation of bone origion hydroxyapatite at elevated temperatures and in selected atmospheres", Advanced Materials Research, 29-30 (2007) 231-234.

ELEKTROPRZĘDZENIE: NANOWŁÓKNA WĘGLOWE Z PREKURSORA POLIAKRYLONITRYLOWEGO MODYFIKOWANEGO HYDROKSYAPATYTEM. BADANIA NAD PROCESEM STABILIZACJI

Izabella Rajzer*, Włodzimierz Biniaś, Janusz Fabia, Dorota Biniaś, Jarosław Janicki

ATH Akademia Techniczno-Humanistyczna w Bielsku-Białej,
Wydział Nauk o Materiałach i Środowisku,
Instytut Inżynierii Tekstyliów i Materiałów Polimerowych,
Zakład Materiałów Polimerowych,
ul. Willowa 2, 43-309 Bielsko-Biała
* e-mail: irajzer@ath.bielsko.pl

Streszczenie

Otrzymane metodą elektroprzędzenia włókniny zbudowane z włókien o wymiarach nanometrycznych naśladować mogą budowę i funkcje naturalnej substancji międzykomórkowej (ECM). Ponadto wytworzone tą metodą podłoża umożliwiają otrzymanie przestrzennej porowatej struktury o dużej powierzchni właściwej i połączonej sieci porów, ułatwiającej wzrost i adhezję komórek.

W pracy zaproponowano metodę otrzymywania bioaktywnych nanowłóknistych podłoży zbudowanych z kompozytowych włókien PAN/n-HAp. Pierwszym etapem otrzymywania nanowłókien węglowych jest proces stabilizacji w atmosferze utleniającej. W celu lepszego zrozumienia zmian zachodzących we włóknach poliakrylonitrylowych poddanych działaniu wysokiej temperatury przeprowadzono badania SEM, DSC i FTIR.

Słowa kluczowe: *nanowłókna węglowe, elektroprzędzenie, proces stabilizacji, hydroksyapatyt*

[Inżynieria Biomateriałów, 86, (2009), 22-27]

Wstęp

W ostatnich czasach technika elektroprzędzenia stała się jedną z najbardziej popularnych i uniwersalnych metod produkcji polimerowych podłoży dla inżynierii tkankowej [1]. Zastosowanie metody elektroprzędzenia w dziedzinie inżynierii tkankowej głównie sprowadza się do formowania włóknin z różnych biomateriałów, które są w stanie naśladować strukturę (fizyczne rozmiary) substancji międzykomórkowej (ECM) [2]. Kość jest nanokompozytem składającym się z miękkiej matrycy hydrożelowej (kolagen, inne białka, woda) oraz twardego nieorganicznego składnika jakim jest hydroksyapatyt ($Ca_{10}(PO_4)_6(OH)_2$). Nanokrystaliczny hydroksyapatyt (długość: 20-80 nm, grubość: 2-5 nm) stanowi 70% tkanki kostnej, pozostałe 30% stanowią białka, również o wymiarach nanometrycznych [3]. Przy projektowaniu materiałów na podłoża tkankowe coraz częściej zwraca się uwagę na tzw. materiały biomimetyczne zbudowane z włókien o średnicy odpowiadającej włóknom kolagenowych, z których zbudowana jest substancja międzykomórkowa (ECM). ECM w naturalnych tkankach sprzyja adhezji, proliferacji i różnicowaniu komórek [4]. Idealne podłoże powinno więc w jak największym stopniu naśladować naturalną ECM.

ELECTROSPINNING: CARBON NANOFIBERS FROM POLYACRYLONITRILE MODIFIED BY NANOHYDROXYAPATITE. STUDY OF STABILIZATION PROCESS

Izabella Rajzer*, Włodzimierz Biniaś, Janusz Fabia, Dorota Biniaś, Jarosław Janicki

ATH University of Bielsko-Biala,
Faculty of Materials and Environmental Sciences,
Institute of Textile Engineering and Polymer Science,
Department of Polymer Materials,
Willowa 2 Street, 43-309 Bielsko-Biała, Poland
* e-mail: irajzer@ath.bielsko.pl

Abstract

The electrospun fabrics with nanoscale fibers diameters mimic morphological nano-features of native extracellular matrix (ECM). Moreover scaffolds fabricated by electrospinning method provide a large surface area, porosity and well interconnected pore network structure to facilitate cell adhesion and growth.

In this paper we have proposed a method to obtain bioactive nanofibrous scaffold consisting of PAN/n-HAp nanofibers. Stabilization process in an oxidative atmosphere, as a first step to obtain carbon nanofibers, was studied in order to better understand morphological rearrangements taking place in PAN fibers subjected to high temperatures. Progress of stabilization and the accompanying morphological changes were monitored through SEM, DSC and FTIR methods.

Keywords: *carbon nanofibers, electrospinning, stabilization process, hydroxyapatite*

[Engineering of Biomaterials, 86 (2009), 22-27]

Introduction

Recently the electrospinning technique is getting one of the most popular and versatile tool for fabrication of polymer scaffolds for tissue engineering [1]. The use of electrospinning in the field of tissue engineering is mainly concentrated towards formation of non-woven mats of different biomaterials to biomimic physical dimensions of native extracellular matrix (ECM) [2]. Bone is a nanocomposite that consists of a protein based soft hydrogel template (i.e., collagen, non-collagenous proteins and water) and hard inorganic components (HAp-hydroxyapatite $Ca_{10}(PO_4)_6(OH)_2$). Specifically, 70% of the bone matrix is composed of nanocrystalline HAp which is typically 20-80 nm long and 2-5 nm thick. Other protein components (30%) in the bone ECM are also nanometer in dimension [3]. It is often beneficial to mimic certain features of a ECM in scaffold design. ECM in natural tissues supports cell attachment, proliferation and differentiation [4]. Ideally the scaffold should mimic natural ECM as much as possible. Therefore within the last years, electrospun nanofibrous scaffolds have been started to be used in tissue engineering application due to their biomimetic character and porous structure [5]. Nonwoven fibrous mats comprised of nanofibers have a very high fraction of surface available to interact with cells, which make them ideal for cell attachment.

Dlatego na przestrzeni ostatnich lat technika elektroprzędzenia została z powodzeniem wykorzystana do otrzymywania nanowłóknistych podłoży dla inżynierii tkankowej ze względu na biomimetyczny charakter i porowatą strukturę otrzymanych w taki sposób materiałów [5]. Włókniny zbudowane z nanowłókien posiadają duży udział powierzchni oddziaływującej na komórki, sprzyjając tym samym ich lepszej adhezji. Dodanie nanowypełniaczy takich jak n-HAp do nanowłóknistej polimerowej matrycy może polepszyć jej mechaniczne czy też inne biologiczne własności niezbędne do zastosowań w inżynierii tkankowej.

W pracy zaproponowano metodę otrzymywania syntetycznych kompozytów zbudowanych z nanocząstek oraz nanowłókien, naśladujących w maksymalny sposób naturalny kompozyt jakim jest kość.

Nanowłókna węglowe (n-CF) cieszą się coraz większym powodzeniem w projektowaniu nowych biomateriałów dla różnych zastosowań medycznych [6-8]. Zastosowanie hydroksyapatytu jako dodatku do nanowłókien węglowych pozwala na uzyskanie podłoża o charakterze bioaktywnym. Tak otrzymany nanokompozyt mógłby w przyszłości zostać wykorzystany jako implant sprzyjający regeneracji tkanki kostnej. Kluczowym procesem otrzymywania włókien węglowych jest proces stabilizacji prowadzony w temperaturze 150-300°C. W pracy przeanalizowano proces stabilizacji kompozytowych nanowłóknin modyfikowanych hydroksyapatytem, stanowiący pierwszy etap w otrzymywaniu bioaktywnych nanowłóknistych podłoży tkankowych.

Materiały i metody

Nanowłókna przygotowano metodą elektroprzędzenia z roztworu poliakrylonitrylu z dodatkiem hydroksyapatytu. Do wytworzenia nanowłókien wykorzystano termopolimer PAN (firmy Zoltek) o składzie: 93-94% wagowych merów akrylonitrylu, 5-6% wagowych merów akrylanu metylu i 1% wagowy merów alilosulfonianu sodowego oraz nano-hydroksyapatyt (średnia wielkość cząsteczek 23 nm, powierzchnia właściwa 81,2 m^2/g) wytworzony w Katedrze Technologii Ceramiki i Materiałów Ogniotrwałych Akademii Górniczo-Hutniczej w Krakowie. Jako rozpuszczalnik zastosowano dimetyloformamid (DMF). Dodatek proszku hydroksyapatytu do roztworu wynosił odpowiednio 3% i 5%. Kompozytowy roztwór polimeru umieszczono w strzykawce (25 ml) o średnicy dyszy 0,5 mm. Proces elektroprzędzenia prowadzono na aparacie własnej produkcji składającym się ze źródła wysokiego napięcia, strzykawki i elektrod (RYS. 1). Odległość pomiędzy elektrodami wynosiła 13,5 cm, wartość przyłożonego napięcia stałego 50 kV. Podczas elektroprzędzenia z roztworu polimeru odparowuje rozpuszczalnik a nanowłókna osadzają się na folii aluminiowej nawiniętej na kręcący się metalowy bęben. W rezultacie otrzymano kompozytową włókninę zbudowaną z nanowłókien PAN/n-HAp. Następnie włókniny poddano procesowi stabilizacji w atmosferze powietrza. Proces utleniania prowadzono wieloetapowo (150°C/1h; 200°C/2h; 220°C/2h; 240°C/2h; 260°C/2h and 280°C/2h).

Mikrostrukturę otrzymanych kompozytowych nanowłóknin PAN/n-HAp oraz sposób rozprowadzenia w nich cząstek hydroksyapatytu scharakteryzowano przy użyciu skaningowej mikroskopii elektronowej (NOVA NANO SEM 200, FEJ EUROPE COMPANY) jak również mikroskopu Jeol, JSM-5400 wyposażonego w mikroanalizator dyspersji energii promieniowania rentgenowskiego EDX Link ISIS 300 z mikroanalizą rentgenowską (Oxford Instrument). Próbki nanowłókien polimerowych (nieprzewodzących) przed obserwacją napylano węglem.

The incorporation of nanofillers such as HAp into the nano scale polymer matrix may gain enhanced mechanical, biological and other related properties for tissue engineering applications.

In the current study we have proposed a method to obtain a synthetic nanocomposites consisting of nanoparticles and nanofibers that maximally mimic the natural composites (i.e. bone).

Carbon nanofibers (n-CF) offer an unusual potential in designing new biomaterials for various medical applications [6-8]. Addition of bioactive fillers such as nanohydroxyapatite into the carbon nanofibers, aims to assure the bioactive behavior of the scaffold. Such nanocomposites have possible prospects for application as bone implant. For converting PAN to carbon fiber, thermo-oxidative stabilization in 150-300°C range is a key step. In this paper we report the properties of thermally oxidized PAN/n-HAp composite nanofibers as first step to obtain bioactive carbon nanofibrous scaffold.

Materials and methods

Nanofibers were prepared by electrospinning from composite polyacrylonitrile/hydroxyapatite solution. Polyacrylonitrile (PAN) - terpolymer (93-94% of weight mers of acrylonitrile, 5-6% of weight mers of methyl acrylate, and about 1% of sodium alilosulphoniane) from Zoltek (Hungary) was used for obtaining the nanofibers. Nano-hydroxyapatite (n-HAp) produced at the Department of Technology of Ceramics and Refractories, AGH-UST (Cracow, Poland) was added to the spin dope. An average size of the n-HAp particles was about 23 nm. The specific surface area of the n-HAp was 81.2 m^2/g.

PAN was dissolved in dimethyl formamide (DMF) and mixed with 3% and 5% of n-HAp respectively to form composite solution. Composite solution was fed through a capillary tip (diameter 0.5 mm) using a syringe (25 ml). Electrospinning was carried out using home-made apparatus consisting of a power supply, syringe and electrodes (FIG. 1). The blend solution was spun at a working distance of 13.5 cm with a driving force of 50 kV. The fibers were dried in flight and collected on the aluminium foil wrapped on a rotating metal drum. Non-woven PAN/n-HAp fabric, was obtained using this method. The electrospun PAN/HAp nanofibers were then stabilized in oxidizing atmosphere by multistage process (150°C/1h; 200°C/2h; 220°C/2h; 240°C/2h; 260°C/2h and 280°C/2h).

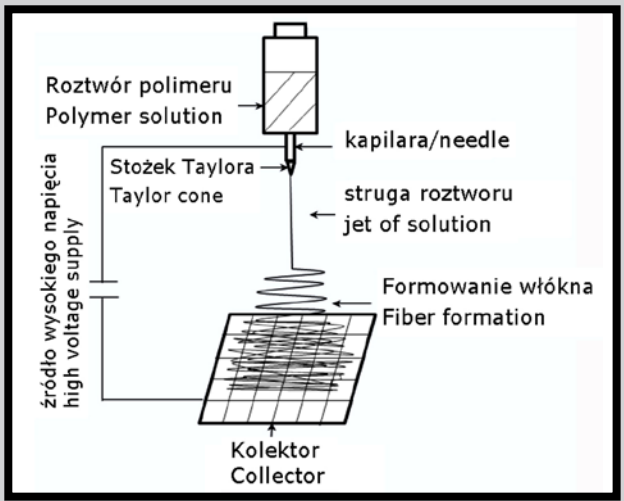

RYS. 1. Schemat urządzenia do otrzymywania włókien metodą elektroprzędzenia.
FIG. 1. Experimental electrospinning set-up.

Badania SEM morfologii włóknin otrzymanych metodą elektroprzędzenia przeprowadzono po każdym z etapów stabilizacji. Stabilność termiczną modyfikowanych nanowłóknin oznaczono na aparacie DSC 5100 firmy TA Instruments. Badania przeprowadzono przy szybkości ogrzewania 10°C/min w atmosferze gazu obojętnego (azot, przy przepływie gazu 40 ml/min). Temperatury pomiaru wynosiły 0-340°C. Zmiany zachodzące w strukturze poliakrylonitrylu podczas procesu stabilizacji włókien określono przy użyciu spektroskopii w podczerwieni. Badania wykonano na aparacie Nicolet 6700 z przystawką dyfuzyjną, w zakresie 400-4000 cm^{-1}.

Wyniki i dyskusja

Na RYS. 2 przedstawiono zdjęcia SEM poliakrylonitrylowych nanowłókien otrzymanych metodą elektroprzędzenia. Obie włókniny składały się z nanowłókien o średnicach w zakresie 100-350 nm. Cząsteczki hydroksyapatytu były równomiernie rozprowadzone na powierzchni włókien, jednocześnie można było również zaobserwować ich aglomeraty (RYS. 2c).

Microstructure of composite PAN/n-HAp nanofibers as well as the distribution of hydroxyapatite particles in the polymer matrix were estimated using scanning electron microscopy (NOVA NANO SEM 200, FEJ EUROPE COMPANY) as well as Jeol, JSM-5400 - equipped with EDX Link ISIS 300 X-ray microanalyser (Oxford Instruments). Polymer nanofibers were sputtered with carbon prior to observation. The morphology of electrospinning nanofibers and nanofibers after each step of stabilization process was compared by SEM method. Thermal stability of modified polyacrylonitrile nano-fibers was estimated by differential scanning calorimetry (DSC) method using 5100 analytical system (TA Instruments), at following conditions: heating rate 10°C/min, nitrogen gas flow (40 ml/min), temperature from 0 to 340°C. The infrared spectroscopy was applied for phase analysis as well as to determine the structural changes of polyacrylonitrile chain structure occurring during thermal stabilization process. IR spectra were recorded with Nicolet 6700 spectrophotometer (4000-400 cm^{-1}) using diffuse reflectance.

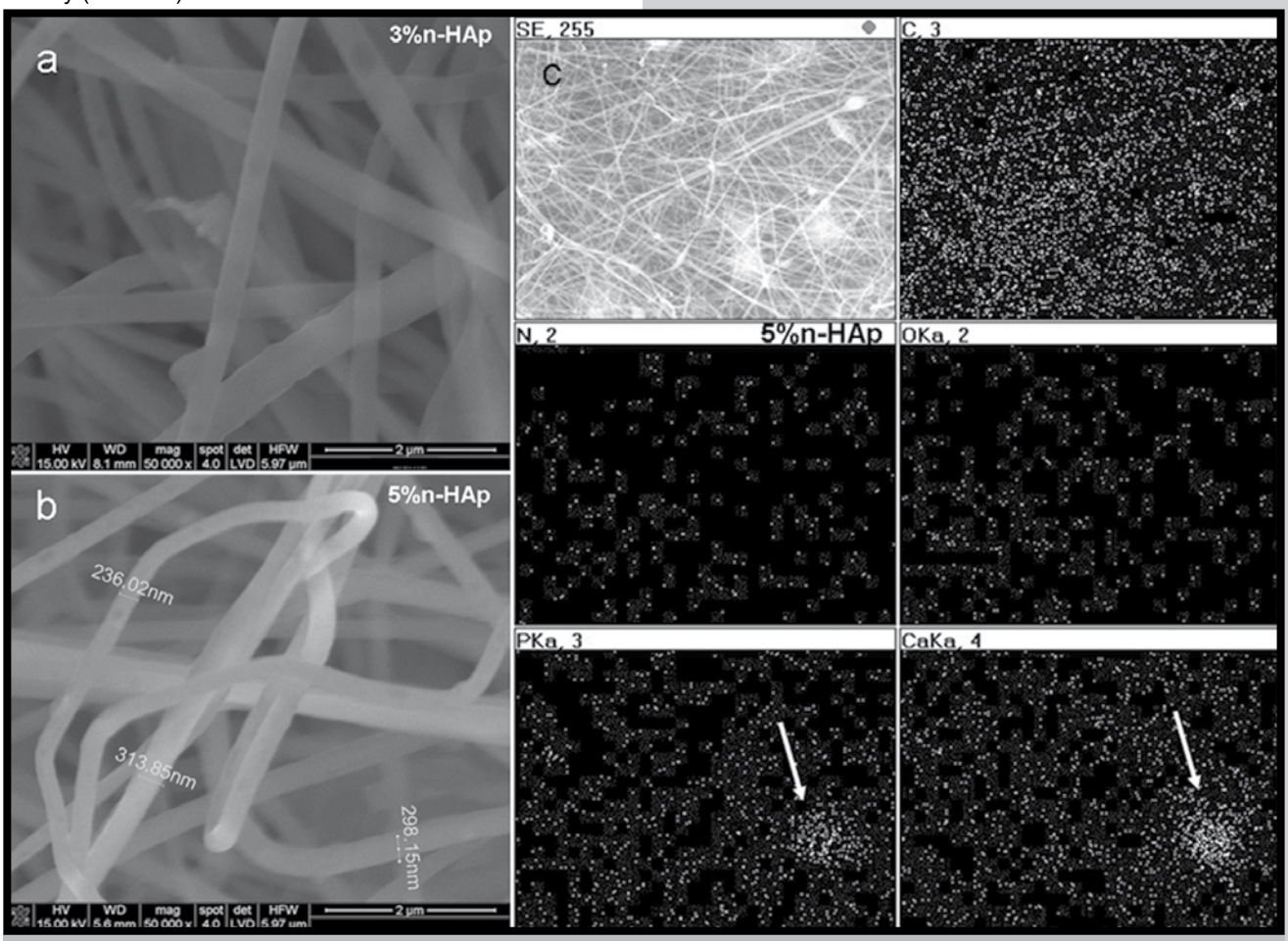

RYS. 2. Mikrostruktura nanowłóknin PAN/n-HAp: a) z dodatkiem 3% n-HAp; b) 5% n-HAp; c) analiza EDX powierzchni nanowłókien kompozytowych modyfikowanych 5% n-HAp.
FIG. 2. Microstructure of PAN/n-HAp nanofabrics: a) with 3% of n-HAp; b) 5% of n-HAp; c) EDX analysis of surfaces of composite PAN nanofibers modified with 5% of hydroxyapatite.

Nanowłókna PAN poddano badaniom DSC w celu określenia wpływu wzrostu temperatury na proces ich utleniania (RYS. 3). Z krzywych DSC wynika, że od 0°C-280°C, obie próbki (PAN/3%n-HAp, PAN/5%n-HAp) są stabilne termicznie, natomiast pik egzotermiczny dla próbek PAN/3%n-HAp, PAN/5%n-HAp występuje odpowiednio w temperaturze 304°C i 310°C. Można zaobserwować niewielki wpływ dodatku hydroksyapatytu na efekt egzotermiczny.

Results and discussions

FIG. 2 shows the SEM images of PAN nanofibers fabricated by electrospinning system. Each nanofabrics consisted of fibers with diameters ranging from 100 nm to 350 nm. n-HAp particles were evenly dispersed on the fibers surface; however some agglomerates were also visible (FIG. 2c).

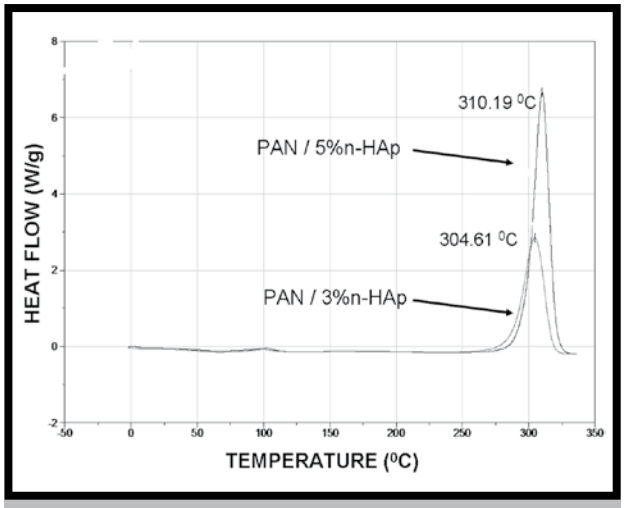

RYS. 3. Zestawienie krzywych DSC dla próbek PAN odpowiednio z zawartością: 3% n-HAp oraz 5% n-HAp.
FIG. 3. DSC curves of PAN samples which contain 3% n-HAp and 5% n-HAp, respectively.

In order to analyze the effect of temperature increase on fibers oxidation, modified precursor nanofibers were analyzed by DSC method (FIG. 3). Both of analyzed samples (PAN/3% n-HAp and PAN/5% n-HAp) were thermally stable up to 300°C and the exothermic peaks were observed at 304°C and 310°C for PAN/3% n-HAp and PAN/5% n-HAp, respectively. It is seen that exothermic effect was little influenced by the addition of n-HAp.

The diameter of fibers decreases during stabilization process (FIG. 4). The fibers with diameter bigger than 300 nm were not observed. During stabilization the color of composite nanofabrics changed from white for the precursor to dark brown for stabilized nanofibers. Analyzing the FTIR spectrum of hydroxyapatite powder (FIG. 5a) one can observe clearly visible bands dedicated to PO_4^{3-} in the 900-1200 cm^{-1} region, the most intensive are attributed to stretching vibrations. Band at 963 cm^{-1} corresponds to non-degenerated symmetric vibrations v_1 P-O. Absorption maxima at 1033 cm^{-1} and 1107 cm^{-1} are attributed to triple-degenerated asymmetric stretching vibrations v_3 P–O, while bands at 566 cm^{-1} and 605 cm^{-1} are attributed to triple-degenerated bending vibrations v_4 O–P–O. FTIR analysis was done also for PAN/n-HAp nanofibers (FIG. 5c, 5d) as well as for unmodified PAN (FIG. 5b). Characteristic FTIR bands of polyacrylonitrile fibers are presented in TABLE 1.

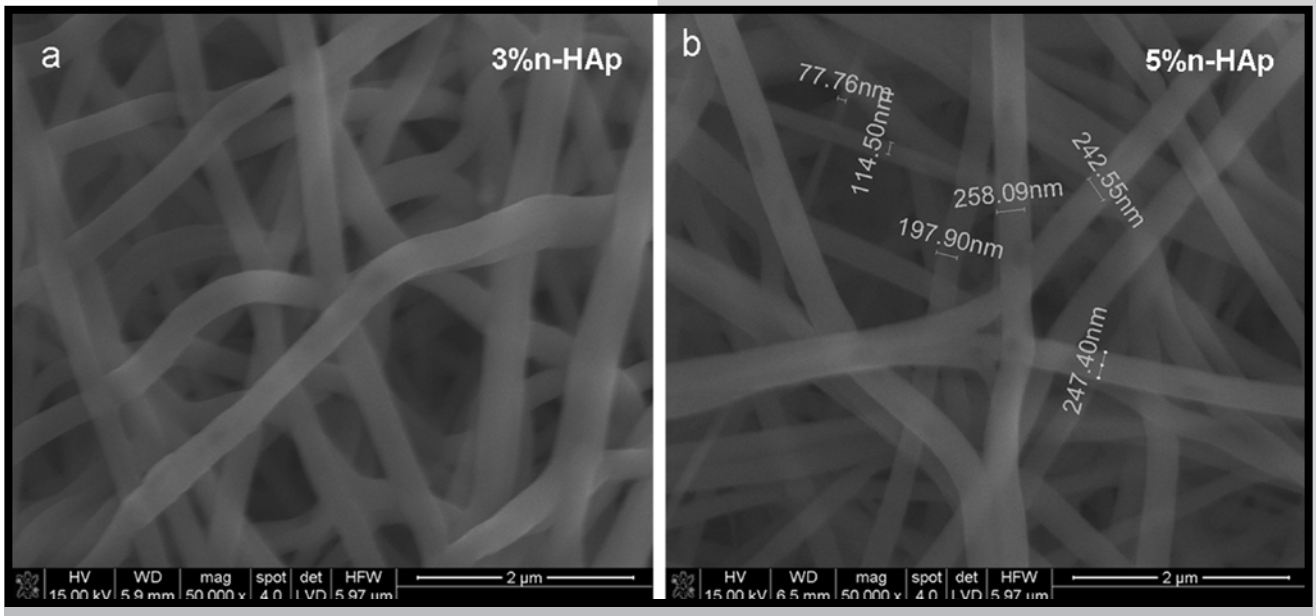

RYS. 4. Mikrostruktura nanowłóknin PAN/n-HAp po procesie stabilizacji: a) z dodatkiem 3% n-HAp; b) 5% n-HAp.
FIG. 4. Microstructure of PAN/n-HAp nanofabrics after stabilization process: a) with 3% of n-HAp; b) 5% of n-HAp.

Ze wzrostem temperatury stabilizacji następuje zmniejszenie średnicy włókien (RYS. 4). W próbkach obserwowanych po procesie stabilizacji brak jest włókien o średnicy większej niż 300 nm. Procesowi stabilizacji prekursora poliakrylonitrylowego towarzyszą również zmiany cech fizycznych polimeru takich jak barwa (biała – prekursor, ciemny brąz – po procesie stabilizacji). Na widmie FTIR proszku hydroksyapatytu (RYS. 5a) wyraźnie widoczne są pasma w zakresie 900-1200 cm^{-1} pochodzące od grup PO_4^{3-}, najintensywniejsze z nich są wynikiem drgań rozciągających. Pasma przy około 963 cm^{-1} pochodzą od niezdegenerowanych symetrycznych drgań v_1 P–O. Maksima absorpcyjne w podczerwieni przy 1033 cm^{-1} jak również 1107 cm^{-1} związane są z potrójnie zdegenerowanymi, antysymetrycznymi drganiami rozciągającymi v_3 P–O. Pasma przy 566 cm^{-1} i 605 cm^{-1} pochodzą od potrójnie zdegenerowanych drgań zginających v_4 O–P–O.

In the case of composite nanofibers regardless of bands characteristic for polymer, there are also observed intensive bands assigned to n-HAp. Important differences were noticed in both cases of modified nanofibers for bands at 1675 cm^{-1} and shoulder band inflection at 1380 cm^{-1} (FIG. 5), and not observed in the case of pure PAN. This differences indicate the presence of the interaction at the molecular level between the nanometric hydroxyapatite fraction and polymer matrix, leading to creation of chemical bonding between n-HAp particles and the polymer chains.

IR analysis was done on each step of thermal stabilization process for both kinds of composite nanofibers (FIG. 6), and the several characteristic changes typical for stabilization of PAN were observed such as decrease in intensity of absorption bands assigned to C-H stretching vibrations (2940 cm^{-1}) and assigned to C≡N group (2240 cm^{-1}). The later evidenced the breakdown of C≡N groups.

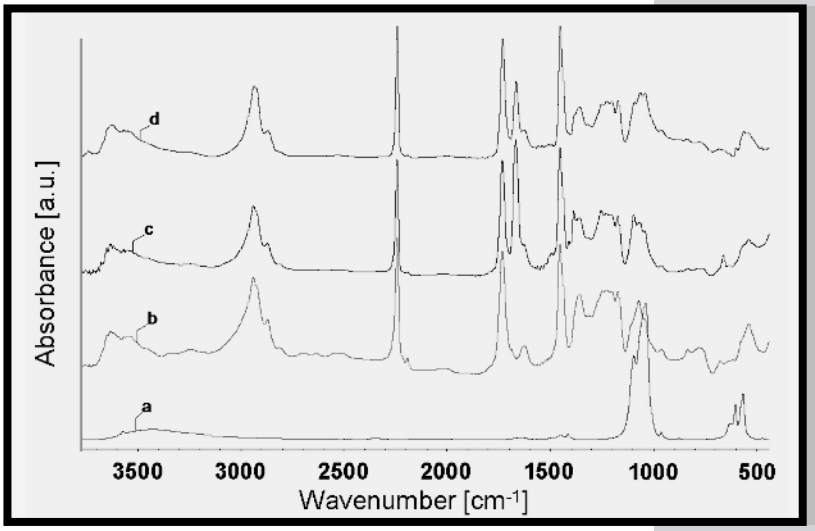

RYS. 5. Widma FTIR kompozytowych włóknin PAN/n-HAp otrzymywanych metodą elektroprzędzenia o różnej zawartości hydroksyapatytu (n-HAp); (a) proszek hydroksyapatytu, (b) PAN, (c) PAN/3%n-HAp, (d) PAN/5%n-HAp.
FIG. 5. FT-IR spectra of electrospun n-HAp/PAN composite fabrics with various n-HAp contents; (a) n-HAp powder, (b) PAN, (c) PAN/3%n-Hap, (d) PAN/5%n-HAp.

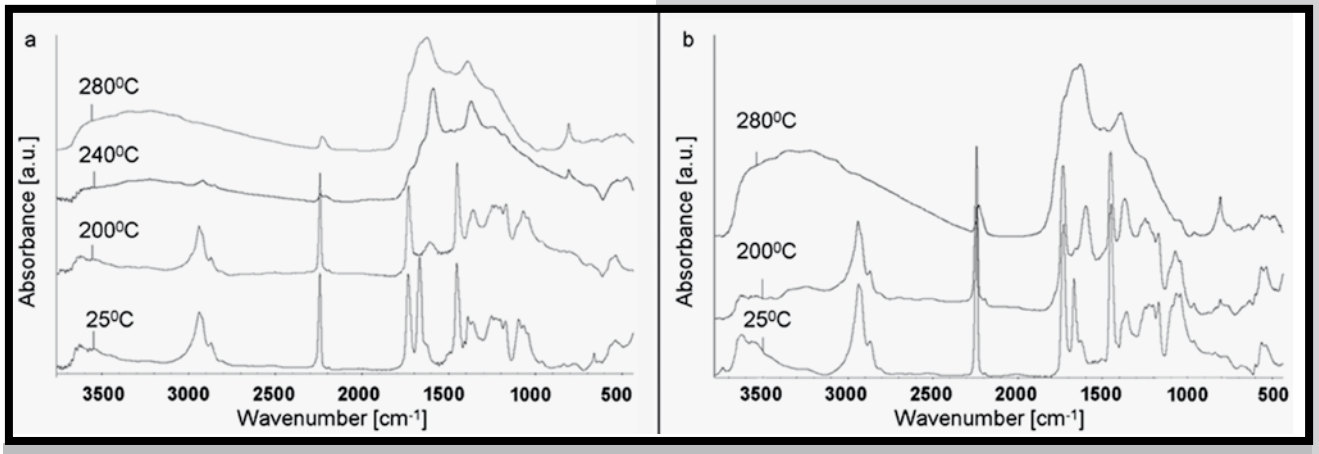

RYS. 6. Widma FTIR kompozytowych włóknin n-HAp/PAN otrzymywanych metodą elektroprzędzenia stabilizowanych w różnych temperaturach (w atmosferze powietrza): (a) PAN/3%n-HAp; (b) PAN/5%n-HAp.
FIG. 6. FT-IR spectra of electrospun n-HAp/PAN composite fabrics thermally treated at various temperatures (air atmosphere): (a) PAN/3%n-HAp; (b) PAN/5%n-HAp.

Przedmiotem badań były również nanowłókniny PAN/n-HAp (RYS. 5c i 5d) jak również niemodyfikowane włókna poliakrylonitrylowe (RYS. 5b). Przyporządkowanie pasm dla nanowłókien poliakrylonitrylowych przedstawiono w TABELI 1. W widmach nanowłókien kompozytowych poza pasmami typowymi dla polimeru widoczne są również intensywne pasma pochodzące od hydroksyapatytu. Jedyne znaczące różnice związane są z pasmem położonym przy 1675 cm^{-1} oraz przegięciem widocznym na zboczu pasma przy 1380 cm^{-1} (RYS. 5), występują one w obu widmach próbek kompozytowych natomiast są niewidoczne w widmach czystego polimeru. Subtelne zmiany obserwowane w widmach IR nanokompozytów w porównaniu do widm czystego polimeru wskazują, że nanometryczna frakcja hydroksyapatytu oddziaływuje z polimerową matrycą na poziomie molekularnym tworząc wiązania chemiczne z łańcuchem polimeru.

Po każdym z etapów stabilizacji wykonano badania w podczerwieni obu nanowłóknin kompozytowych (RYS. 6). W obrazach widm obserwuje się zmiany charakterystyczne dla procesu stabilizacji poliakrylonitrylu, a mianowicie: zmniejszenie intensywności pasm absorpcyjnych wywołanych drganiami rozciągającymi C-H (2940 cm^{-1}) oraz spadek intensywności pasma absorpcyjnego związanego z drganiami grup nitrylowych C≡N (2240 cm^{-1}). Obniżenie intensywności tego pasma świadczy o rozpadzie grup C≡N. Jednocześnie tworzą się nowe pasma: przy 1600 cm^{-1} (drgania rozciągające grupy C=C i C=N), szerokie pasmo w zakresie 1000 cm^{-1} – 1500 cm^{-1} i słabe pasmo przy 800 cm^{-1} (drgania deformacyjne C-H).

TABELA 1. Przypisanie pasm w widmie w podczerwieni poliakrylonitrylu.
TABLE 1. FTIR bands of polyacrylonitrile fibers.

Liczba falowa Wavenumber [cm^{-1}]	Drgania Vibrations	Rodzaj wiązania Type of bond
3500	stretching rozciągające	O-H
3200-3700	stretching rozciągające	N-H, NH_2
2940	stretching rozciągające	C-H
2920	stretching rozciągające	CH_2
2240	stretching rozciągające	C≡N
1730	stretching rozciągające	C=O
1650	stretching rozciągające	C=C
1450,1360	deformation deformacyjne	CH_2, CH_3
1380	bending zginające	CH, NH
1250	stretching rozciągające	C-N or C-C

Pasmo w położeniu 1730 cm^{-1} (C=O) w widmach utlenianych włókien zwiększa szerokość połówkową w miarę ogrzewania próbek, a następnie po przekroczeniu temperatury 220°C staje się niewidoczne. Końcowej stabilizacji włókien towarzyszy całkowity zanik pasm przy 2940 cm^{-1} i 1730 cm^{-1} oraz pojawienie się szerokiego pasma w zakresie 1000 cm^{-1}-1500 cm^{-1} w widmach IR analizowanych materiałów. W temperaturze 280°C widma obu próbek były identyczne, natomiast obecne jest nadal pasmo pochodzące od drgań grup nitrylowych (2240 cm^{-1}) charakterystycznych dla PAN, którego obecność świadczy o tym, że proces stabilizacji nie jest jeszcze zakończony. Porównanie wyników badań FTIR i DSC ukazuje, że obniżenie intensywności pasma pochodzącego od drgań grup (-C≡N) jest bezpośrednio związane z obecnością piku egzotermicznego w zakresie temperatur 304-310°C. Dlatego aby proces stabilizacji był przeprowadzony w pełni próbki należy stabilizować do temperatury 300°C.

Wnioski

Stosując metodę elektroprzędzenia z powodzeniem otrzymano kompozytowe nanowłókniny PAN/n-HAp. Zaobserwowano, że cząsteczki n-HAp były zdyspergowane w matrycy polimerowej. Modyfikacja nanowłókien poliakrylonitrylowych hydroksyapatytem i ich późniejsza stabilizacja stwarza możliwość użycia tak wytworzonego materiału jako bioaktywnego podłoża do regeneracji tkanki.

Podziękowania

Autorzy chcieliby złożyć najserdeczniejsze podziękowania Pani Prof. A. Ślósarczyk oraz Pani Dr A. Zimie (AGH-UST Kraków) za udostępnienie proszku hydroksyapatytu, jak również Panu Dr M. Boguniowi (Politechnika Łódzka) za dostarczenie proszku poliakrylonitrylu.

Praca naukowa finansowana ze środków na naukę w latach 2007-2010 jako projekt badawczy POL-POSTDOC III Nr PBZ/MNiSW/07/2006/53.

Simultaneously new bands appeared at 1600 cm^{-1} (C=C and C=N stretching vibrations); at a region 1000 cm^{-1}-1500 cm^{-1} and weak band at 800 cm^{-1} (C-H deformations). Along with the oxidation process the half width of band assigned to carbonyl group C=O (1730 cm^{-1}) was increasing and then above 220°C disappeared. The last stage of stabilization process was accompanied with disappearance of bands at 2940 cm^{-1} and 1730 cm^{-1} and appearance of wide band at 1000 cm^{-1}-1500 cm^{-1} range. At 280°C spectra of both types of nanofibrics were identical but there was still some evidence of bands assigned to nitrille groups (2240 cm^{-1}) typical for PAN macromolecules, which indicated that the stabilization process was not totally completed. The correlation of the FTIR result with the DSC behaviour reveals the decrease of the -C≡N groups is directly related to the exothermic peak at c.a. 304-310°C. Therefore further stabilization at 300°C should be done.

Conclusions

Nanocomposites of PAN/n-HAp were successfully produced by electrospinning. It was observed that n-HAp nanoparticles were dispersed inside PAN matrix within the scaffold. The successful modification of the polyacrylonitrile nano-fibers with the hydroxyapatite and its subsequent stabilization create an opportunity to use these nanofibers as bioactive scaffold for tissue regeneration.

Acknowledgments

The authors would like to thank Prof. A. Ślósarczyk and Dr A. Zima (AGH-UST Cracow) for providing n-HAp powder as well as Dr M. Boguń (Technical University of Lodz) for providing the PAN polymer powder.

This work was supported by the Minister of Science and Higher Education; project POL-POSTDOC III no. PBZ/MNiSW/07/2006/53 (2007-2010).

Piśmiennictwo

[1] Sill TJ, Von Recum HA. Electrospinning: Applications in drug delivery and tissue engineering. Biomaterials 2008; 29: 1989-2006.
[2] Agarwal S, Wendorff JH, Greiner A. Use of electrospinning technique for biomedical applications. Polymer 2008; 49: 5603-5621.
[3] Zhang L, Webster TJ. Nanotechnology and nanomaterials: Promises for improved tissue regeneration. Nano Today 2009; 4:66-80.
[4] Liao S, Chan CK, Ramakrishna S. Stem cells and biomimethic materials strategies for tissue engineering. Materials Science and Engineering C 2008; 28: 1189-1202.
[5] Murugan R., Ramakrishna S. Nano-Featured Scaffolds for Tissue Engineering: A Review of Spinning Methodologies. Tissue Engineering 2006; 12 (3): 435-448.

References

[6] McKenzie JL, Waid MC, Shi R, Webster TJ. Decreased functions of astrocytes on carbon nanofiber materials. Biomaterials 2004; 25: 1309-1317.
[7] Price RL, Waid MC, Haberstroh KM, Webster TJ. Selective bone ell adhesion on formulations containing carbon nanofibers. Biomaterials 2003; 24: 1877-1887.
[8] Elias KL, Price RL, Webster TJ. Enhanced functions of osteoblasts on nanometer diameter carbon fibers. Biomaterials 2002; 23: 3279-3287.

BADANIA CENTRÓW PARAMAGNETYCZNYCH MELANINY Z SEPIA OFFICINALIS METODĄ EPR

Ewa Chodurek[1], Daria Czyżyk[2], Barbara Pilawa[2], Sławomir Wilczyński[2]

[1] Katedra i Zakład Biofarmacji, Wydział Farmaceutyczny z Oddziałem Medycyny Laboratoryjnej w Sosnowcu, Śląski Uniwersytet Medyczny w Katowicach, ul. Narcyzów 1, 41-200 Sosnowiec
[2] Katedra i Zakład Biofizyki, Wydział Farmaceutyczny z Oddziałem Medycyny Laboratoryjnej w Sosnowcu, Śląski Uniwersytet Medyczny w Katowicach, ul. Jedności 8, 41-200 Sosnowiec

Streszczenie

Przeprowadzono badania właściwości paramagnetycznych biopolimeru melaninowego otrzymanego z Sepia officinalis z zastosowaniem spektroskopii elektronowego rezonansu paramagnetycznego na pasmo X (9,3 GHz). Biopolimer ten jest wykorzystywany w preparatach kosmetycznych. Analizowano kształt i parametry widm EPR centrów paramagnetycznych melaniny zarejestrowanych jako pierwsza pochodna absorpcji. Otrzymano wartości współczynnika rozszczepienia spektroskopowego g, amplitudy, intensywności integralnej i szerokości linii EPR. Wyznaczono koncentrację centrów paramagnetycznych w badanym biopolimerze melaninowym. Stwierdzono podobne widma EPR i właściwości centrów paramagnetycznych melaniny z Sepia officinalis oraz eumaleniny.

Zależne od mocy mikrofalowej asymetryczne widma EPR wskazują na złożony charakter układu centrów paramagnetycznych w testowanym biopolimerze. Wykazano, że w melaninie z Sepia officinalis występują głównie o-semichinonowe wolne rodniki. Wolne procesy relaksacji spin-sieć zachodzą w analizowanej melaninie.

Słowa kluczowe: *biopolymer melaninowy, Sepia officinalis, centra paramagnetyczne, wolne rodniki, EPR*

[Inżynieria Biomateriałów, 86, (2009), 28-32]

Wprowadzenie

Melaniny są biopolimerami wykazującymi właściwości paramagnetyczne [1-12]. o-Semichinowe wolne rodniki z niesparowanymi elektronami zlokalizowanymi na atomie tlenu głównie odpowiadają za paramagnetyzm melanin [1-12]. Techniką przydatną do badania tych naturalnych polimerów jest elektronowy rezonans paramagnetyczny. Porównanie widm EPR kompleksów melanin z jonami metali wykazało, że dia- i paramagnetyczne jony metali odpowiednio zwiększają lub zmniejszają koncentrację wolnych rodników w melaninie [1,3-4,8,11-13,25]. Badania EPR wskazują na istotną rolę melaninowych centrów paramagnetycznych w wiązaniu substancji leczniczych [13-16] oraz jonów metali [1,3-4,7-8,11-13,15] do tych polimerów. Wolne rodniki melanin mogą powodować efekty toksyczne w tkankach [18-19].

EPR STUDIES OF PARAMAGNETIC CENTERS IN MELANIN FROM SEPIA OFFICINALIS

Ewa Chodurek[1], Daria Czyżyk[2], Barbara Pilawa[2], Sławomir Wilczyński[2]

[1] Department of Biopharmacy, School of Pharmacy and Laboratory Medicine, Medical University of Silesia in Katowice, 1 Narcyzów Str., 41-200 Sosnowiec, Poland
[2] Department of Biophysics, School of Pharmacy and Laboratory Medicine, Medical University of Silesia in Katowice, 8 Jedności Str., 41-200 Sosnowiec, Poland

Abstract

Paramagnetic properties of melanin biopolymer from Sepia officinalis were studied by the use of electron paramagnetic resonance spectroscopy (EPR) at X-band (9.3 GHz). This biopolymer is applied in cosmetics. Lineshape and parameters of first-derivative EPR spectra of melanin paramagnetic centers were analysed. g-Factor, amplitude, integral intensity, and linewidth of EPR spectra were obtained. Concentration of paramagnetic centers in melanin biopolymer was determined. EPR spectra of melanin from Sepia officinalis and properties of its paramagnetic centers are similar to those of eumelanin.

Asymmetrical EPR spectra dependent on microwave power indicate that complex paramagnetic centers system is characteristic for the tested biopolymer. It was proved that mainly o-semiquinone free radicals exist in melanin from Sepia officinalis. Slow spin-lattice relaxation processes exist in the analysed melanin.

Keywords: *melanin biopolymer, Sepia officinalis, paramagnetic centers, free radicals, EPR*

[Engineering of Biomaterials, 86 (2009), 28-32]

Introduction

Melanins are paramagnetic biopolymers [1-12]. o-Semiquinone free radicals with unpaired electron localized on oxygen atom are mainly responsible for paramagnetism of melanins [1-12]. Electron paramagnetic resonance spectroscopy is a useful technique to examine of these natural polymers. Comparison of EPR spectra of melanin complexes with metal ions indicates that dia- and paramagnetic metal ions increase and decrease free radical concentration in melanin, respectively [1,3-4,8,11-13,25]. EPR studies indicate that melanin's paramagnetic centers play an important role in binding of drugs [13-16] and metal ions to this polymer [1,3-4,7-8,11-13,15]. Free radicals may be responsible for toxic effects in tissues [18-19].

EPR studies of melanin from Drosophila melanogaster (the strains: black, grey, and yellow), Cladosporium cladosporiodes and Cladosporium herbarum were performed by us earlier [7,9,26]. In these works we concentrated on the role of melanin's free radicals in environmental protection, detoxification processes and type of melanin existing in the mentioned above biological objects.

Badania EPR melanin z Drosophila melanogaster (szczep: czarny, szary i żółty), Cladosporium cladosporiodes i Cladosporium herbarum przeprowadziliśmy wcześniej [7,9,26]. W powyższych pracach koncentrowaliśmy się głównie na roli wolnych rodników melaniny w ochronie środowiska, procesach detoksyfikacji i rodzaju melaniny występującej we wspomnianych powyżej obiektach biologicznych.

W pracy [17] opisano centra paramagnetyczne występujące w całej gamma napromieniowanej Sepia offcinalis. Widma EPR wykorzystano do identyfikacji napromieniowanej mątwy [17]. Melanina występuje także w Sepia officinalis, jednakże nie przeprowadzono badań spektroskopowych jej centrów paramagnetycznych. Celem naszej pracy jest wyznaczenie koncentracji i właściwości centrów paramagnetycznych biopolimeru melaniny z Sepia officinalis. Melanina z Sepia officinalis jest stosowana w kosmetykach, substancjach leczniczych w kosmetologii i medycynie estetycznej [20-21]. W niniejszej pracy spektroskopię elektronowego rezonansu paramagnetycznego zaproponowano jako metodę użyteczną w badaniach melanin w kosmetykach. Metodą EPR można badać powstawanie wolnych rodników w próbkach kosmetyków zawierających melaninę. Badania EPR melaniny z Sepia offcinalis są ważne, ze względu na potencjalne negatywne efekty w tkankach spowodowane przez oddziaływania tkanki z wolnymi rodnikami melaniny występującej w kosmetykach.

Materiał i metody

Materiał

Biopolimer melaninowy izolowany z Sepia officinalis badano z zastosowaniem spektroskopii EPR. Próbki otrzymano z Firmy Sigma. Próbki melaninowe umieszczono w cienkościennych rurkach szklanych i rejestrowano widma EPR.

Metody

Metodę elektronowego rezonansu paramagnetycznego (EPR) o częstotliwości promieniowania mikrofalowego z pasma X wynoszącej 9,3 GHz zastosowano jako technikę eksperymentalną. Widma EPR mierzono za pomocą spektrometru RADIOPAN (Poznań) w szerokim zakresie mocy mikrofalowej wynoszącym 0,7-70 mW. Widma EPR w postaci pierwszej pochodnej rejestrowano w temperaturze pokojowej. Analizowano następujące parametry kształtu linii EPR: A_1/A_2, A_1-A_2, B_1/B_2 i B_1-B_2. Parametry te zdefiniowano na RYS. 1. Dla widm eksperymentalnych wyznaczono współczynnik rozszczepienia spektroskopowego g, amplitudę (A), intensywność integralną (I) oraz szerokość linii (ΔB_{pp}). Zbadano wpływ mocy mikrofalowej na parametry asymetrii linii oraz na amplitudę i szerokość linii EPR.

Współczynnik rozszczepienia spektroskopowego g obliczono z warunku rezonansu jako $hv/\mu_B B_r$, gdzie: h – stała Plancka, v – częstotliwość mikrofalowa, μ_B – magneton Bohra, B_r - rezonansowa indukcja magnetyczna [22-23]. Koncentrację centrów paramagnetycznych w testowanym biopolimerze wyznaczono jako wielkość proporcjonalną do intensywności integralnej. Jako wzorce wykorzystano ultramarynę i kryształ rubinu.

Wyniki i dyskusja

W przypadku badanego biopolimeru melaninowego z Sepia officinalis rejestrowano silne widma EPR w całym zakresie mocy mikrofalowej (0,7-70 mW). Widma EPR testowanej melaniny stanowią pojedyncze asymetryczne linie (RYS. 1). Kształt tych widm EPR jest podobny do kształtu linii EPR modelowej eumelaniny – DOPA-melaniny.

Paramagnetic centers in whole gamma irradiated Sepia offcinalis are described in work [17]. EPR spectra are used for identification of irradiated cuttlefish [17]. Melanin also exists in Sepia officinalis, but its paramagnetic centers were not analysed spectroscopically. The aim of our work is to determine concentration and properties of paramagnetic centers in melanin biopolymer isolated from Sepia officinalis. Melanin from Sepia officinalis is used in cosmetics and drugs in cosmetology and esthetical medicine [20-21]. In this work electron paramagnetic resonance spectroscopy is proposed as the useful method of study melanin in cosmetics. Free radicals formation in cosmetic samples containing melanin may be examined by EPR method. The EPR studies of melanin from Sepia offcinalis are important, because of potential negative effects caused by their free radicals in tissues during interactions with cosmetics.

Material and methods

Material

Melanin biopolymer isolated from Sepia officinalis was studied by EPR spectroscopy. The samples were obtained from Sigma Firm. Melanin samples were put into thin walled glass tubes and EPR spectra were measured.

Methods

Electron paramagnetic resonance spectroscopy (EPR) with microwave frequency 9.3 GHz (X-band) was applied as the experimental technique. EPR spectra were measured with microwave powers of 0.7-70 mW by RADIOPAN (Poznań) spectrometer. First derivative EPR spectra were recorded at room temperature. The following shapes parameters were analysed: A_1/A_2, A_1-A_2, B_1/B_2 and B_1-B_2. The parameters are defined and shown in FIG. 1. For the experimental spectra g-factor, amplitude (A), integral intensity (I), and linewidth (ΔB_{pp}) were evaluated. Influence of microwave power on asymmetry parameters, and amplitude and linewidth was examined.

g-Factor was calculated from resonance condition as $hv/\mu_B B_r$, where: h – Planck constant, v – microwave frequency, μ_B - Bohr magneton, B_r,- resonance magnetic field [22-23]. Concentration of paramagnetic centers in the studied biopolymer was determined as the value proportional to integral intensity (I) of its EPR spectra. Ultramarine and a ruby crystal were used as the references.

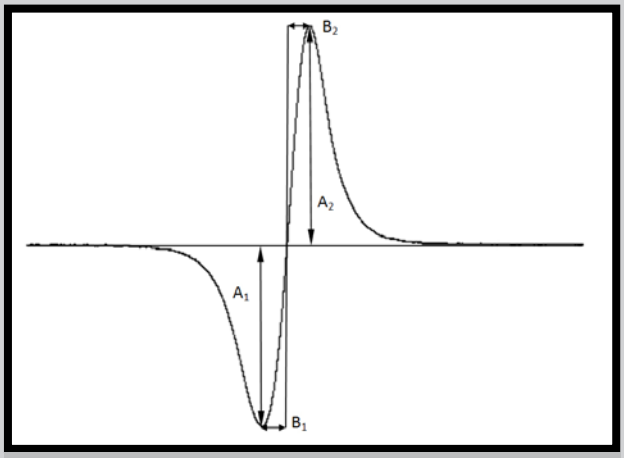

RYS. 1. Widmo EPR biopolimeru melaninowego z *Sepia officinalis* z zaznaczonymi analizowanymi parametrami kształtu linii.
FIG. 1. EPR spectrum of melanin biopolymer from *Sepia officinalis* with marked the analysed parameters of its lineshape.

Widma EPR DOPA-melaniny są również pojedynczymi liniami [1-5,12-16]. Struktura nadsubtelna charakterystyczna dla feoemlanin [2] nie była obserwowana w widmach EPR melaniny z Sepia officinalis. Można więc stwierdzić, że w Sepia officinali występuje eumelanina.

Melaninę z Sepia officinalis charakteryzuje stabilny paramagnetyzm. Linie EPR tego biopolimeru nie zmieniają się z czasem przechowywania próbki. Koncentracja centrów paramagnetycznych w badanej melaninie wynosi $3,2x10^{19}$ spin/g, a współczynnik rozszczepienia spektroskopowego g jest równy 2,0045. Wielkości te są podobne jak dla DOPA-melaniny [1-5,12-16].

W tej pracy wykazano złożony charakter układu centrów paramagnetycznych melaniny z Sepia officinalis. Złożone widma EPR wykazują zmiany asymetrii ze wzrostem mocy mikrofalowej [23]. Wpływ mocy mikrofalowej na parametry asymetrii linii: A_1/A_2, A_1-A_2, B_1/B_2 i B_1-B_2 zdefiniowane na RYS. 1 pokazano odpowiednio na RYS. 2-5.

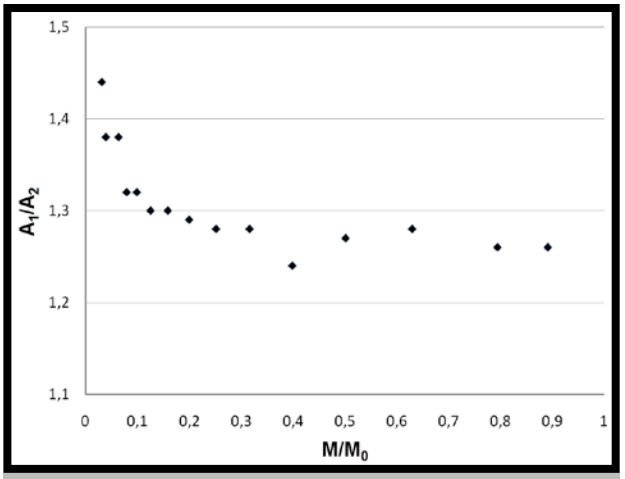

RYS. 2. Wpływ mocy mikrofalowej (M/M_o) na parametr A_1/A_2 widma EPR melaniny z *Sepia officinalis.* M – moc mikrofalowa stosowana podczas pomiaru, M_o – całkowita moc mikrofalowa wytwarzana przez klistron (70 mW).
FIG. 2. Influence of microwave power (M/M_o) on the parameter A_1/A_2 of the melanin's EPR spectra. M – microwave power used during the measurement, M_o – total microwave power produced by klystron (70 mW).

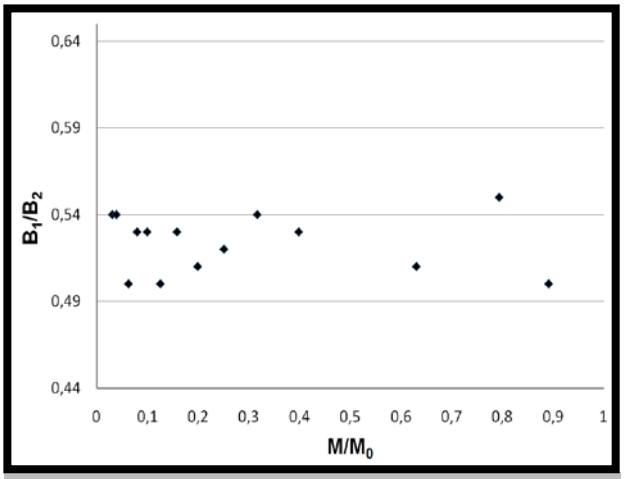

RYS. 4. Wpływ mocy mikrofalowej (M/M_o) na parametr B_1/B_2 widma EPR melaniny z *Sepia officinalis.*
FIG. 4. Influence of microwave power (M/M_o) on the parameter B_1/B_2 of the melanin's EPR spectra.

Results and discussions

Strong EPR spectra in the whole range of microwave power (0.7-70 mW) were measured for the studied melanin biopolymer from Sepia officinalis. The EPR spectra are single asymmetric curves (FIG. 1). Lineshape of these EPR spectra is similar to those of model eumelanin – DOPA-melanin. EPR spectra of DOPA-melanin are single lines [1-5,12-16]. Hyperfine structure characteristic for pheomelanins [2] was not observed in the spectra of melanin from Sepia officinalis. As one can see, eumelanin exists in Sepia officinalis.

Stable paramagnetism characterizes melanin from Sepia officinalis. EPR lines do not change with storage time of the sample. Paramagnetic centers concentration in this melanin is $3.2x10^{19}$ spin/g and g-value is 2.0045. The mentioned above values correspond to those for DOPA-melanin [1-5,12-16].

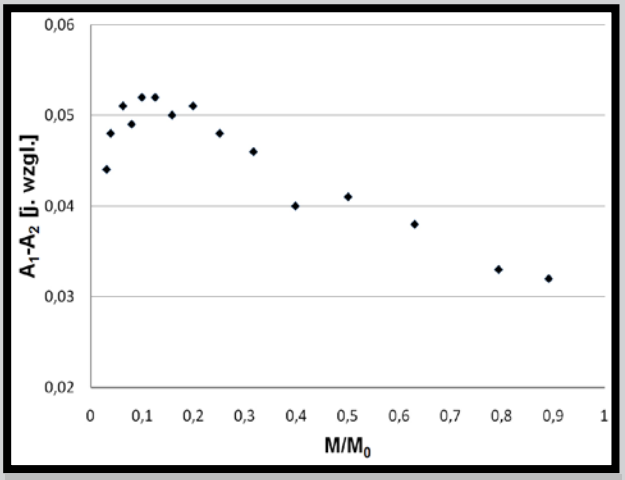

RYS. 3. Wpływ mocy mikrofalowej (M/M_o) na parametr A_1-A_2 widma EPR melaniny z *Sepia officinalis.* M – moc mikrofalowa stosowana podczas pomiaru, M_o – całkowita moc mikrofalowa wytwarzana przez klistron (70 mW).
FIG. 3. Influence of microwave power (M/M_o) on the parameter A_1-A_2 of the melanin's EPR spectra. M – microwave power used during the measurement, M_o – total microwave power produced by klystron (70 mW).

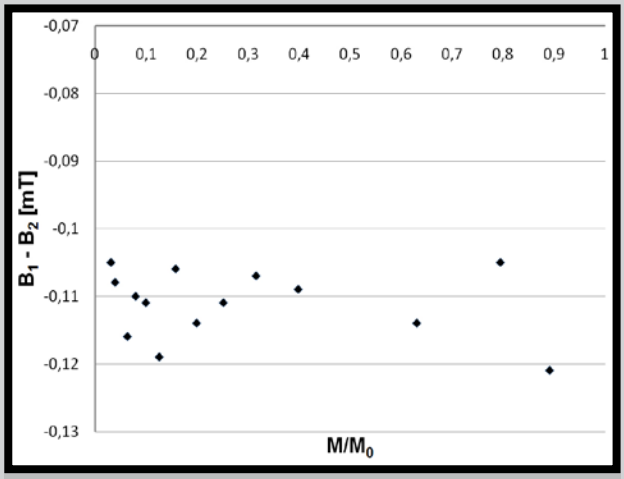

RYS. 5. Wpływ mocy mikrofalowej (M/M_o) na parametr B_1-B_2 widma EPR melaniny z *Sepia officinalis.*
FIG. 5. Influence of microwave power (M/M_o) on the parameter B_1-B_2 of the melanin's EPR spectra.

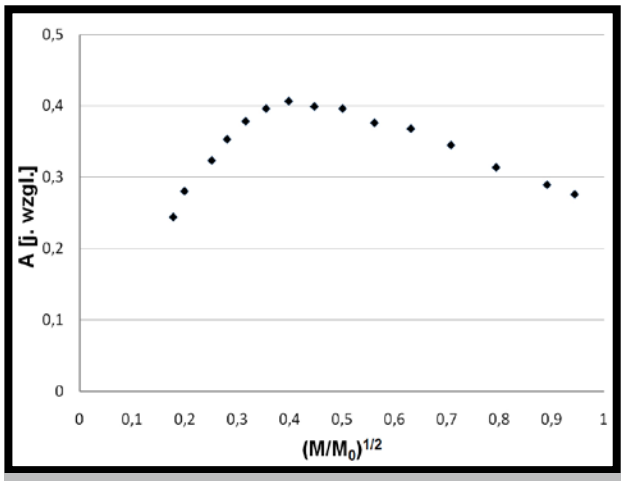

RYS. 6. Wpływ mocy mikrofalowej (M/M_o) na amplitudę A widma EPR melaniny z *Sepia officinalis.*
FIG. 6. Influence of microwave power (M/M_o) on amplitude A of the melanin's EPR spectra.

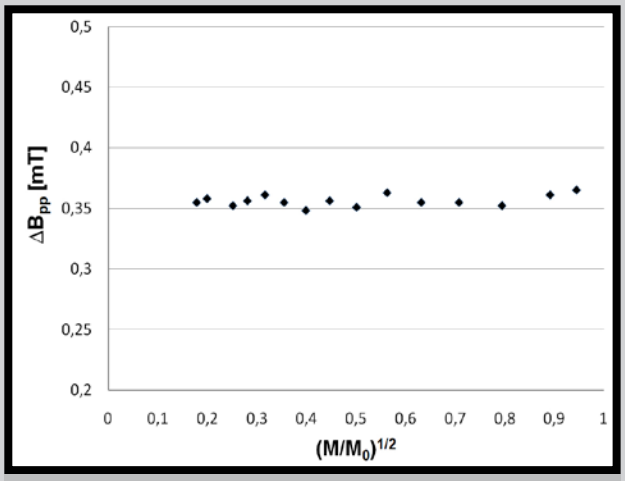

FIG. 7. Wpływ mocy mikrofalowej (M/M_o) na szerokość linii ΔB_{pp} widma EPR melaniny z *Sepia officinalis.*
FIG. 7. Influence of microwave power (M/M_o) on linewidth ΔB_{pp} of the melanin's EPR spectra.

Parametry te znacznie zmieniają się z mocą mikrofalową. Charakter tych zmian pokazano na RYS. 2-5. Podobne zmiany nie wystąpiłyby w próbkach posiadających tylko jeden rodzaj centrów paramagnetycznych [23]. Prawdopodobnie wolne rodniki ze spinem S = 1/2 i dodatkowo birodniki ze spinem S = 1 występują w melaninie z Sepia officinalis. Wolne rodniki i birodniki znaleziono wcześniej w DOPA-melaninie [24-25] i w melaninie z czarnego szczepu Drosophila melanogaster [10,26].

Zmiany amplitudy i szerokości linii analizowanych widm EPR wraz ze wzrostem mocy mikrofalowej pokazano na RYS. 6 i 7. Amplituda linii EPR rośnie wraz ze wzrostem mocy mikrofalowej, a po osiągnięciu wartości maksymalnej maleje z dalszym wzrostem mocy mikrofalowej (RYS. 6). Linie EPR nasycają się dla niskich mocy mikrofalowych (RYS. 6), a więc wolne procesy relaksacji spin-sieć występują w badanej melaninie. Wolne procesy relaksacji spin-sieć zachodzą również w DOPA-melaninie [12-15,24-25], melaninie z Drosophila melanogaster [26] i melaninie z Cladosporium cladosporioides [8-9]. Obserwowano poszerzenie linii EPR ze wzrostem mocy mikrofalowej (RYS. 7). Korelacje przedstawione na RYS. 6 i 7 są charakterystyczne dla linii EPR poszerzonych jednorodnie [22-23]. W próbkach o liniach EPR poszerzonych jednorodnie nie występują izolowane pakiety spinowe [22-23]. Jednorodne poszerzenie linii EPR stwierdzono wcześniej dla DOPA-melaniny [12-15,24-25], melaniny z Drosophila melanogaster [26] i z Cladosporium cladosporioides [8-9].

Wnioski

Badania biopolimeru melaninowego z Sepia officinalis metodą EPR wykazały, że:
1) Silny i stabilny paramagnetyzm charakteryzuje ten polimer podobnie jak eumelaninę.
2) Złożony układ centrów paramagnetycznych występuje w badanym biopolimerze melaninowym wykazującym asymetryczne widma EPR o kształcie zależnym od mocy mikrofalowej.
3) o-Semichinonowe wolne rodniki o współczynniku rozszczepienia spektroskopowego g wynoszącym 2,0045 są głównie odpowiedzialne za widma EPR badanego polimeru.

In this study complex character of paramagnetic centers in melanin from Sepia officinalis is shown. Complex EPR spectra reveal changes of their asymmetry with increasing of microwave power [23]. Influence of microwave power on asymmetry parameters: A_1/A_2, A_1-A_2, B_1/B_2 and B_1-B_2 defined in FIG. 1 is presented in FIG. 2-5, respectively. All these parameters strongly change with microwave power. Character of these changes is presented in FIG. 2-5. Such changes are not obtained for samples with only one group of paramagnetic centers [23]. Probably free radicals with spin S = 1/2 and additionally biradicals with spins S = 1 exist in melanin from Sepia officinalis. Free radicals and biradicals were found in DOPA-melanin [24-25] and in melanin from black strain of Drosophila melanogaster [10,26].

Changes of amplitude and linewidth of the analysed EPR spectra with increasing of microwave power are shown in FIG. 6 and 7, respectively. The amplitude increases with increasing of microwave power, and after reaching the maximum decreases for higher microwave powers (FIG. 6). These EPR lines saturate at low microwave powers, so it can be concluded that slow spin-lattice relaxation processes characterize the studied melanin. Similar slow spin-lattice relaxation processes exist in DOPA-melanin [12-15,24-25], melanin from Drosophila melanogaster [26] and melanin from Cladosporium cladosporioides [8-9]. Broadening of EPR lines with increasing of microwave power we observed (FIG. 7). Correlations presented in FIG. 6 and 7 are characteristic for homogeneously broadened EPR lines [22-23]. Isolated spin packet do not exist in samples with homogeneously broadened EPR lines [22-23]. Homogeneous broadening of EPR lines was obtained for DOPA-melanin [12-15,24-25], melanin from Drosophila melanogaster [26] and Cladosporium cladosporioides [8-9].

Conclusions

EPR studies of melanin biopolymer from Sepia officinalis indicate that:
1) Strong and stable paramagnetism similar to those of eumelanin characterizes this polymer.
2) Complex paramagnetic centers system with asymmetrical EPR spectra, which change with microwave power, exists in the studied melanin biopolymer.
3) o-Semiquinone free radicals with g-factor of 2.0045 are mainly responsible for EPR spectra of the examined polymer.

4) Widma EPR badanej melaniny są poszerzone jednorodnie.
5) Ciągłe nasycenie mikrofalowe linii EPR wskazuje na wolne procesy relaksacji spin-sieć zachodzące w analizowanej próbce melaninowej.
6) Wolne rodniki melaniny izolowanej z Sepia officinalis stosowanej w kosmetykach mogą prawdopodobnie powodować efekty toksyczne w ludzkich tkankach.
7) Przypuszczalnie oddziaływania wolnych rodników melaniny z molekułami tlenu O_2 niszczą strukturę kosmetyków podczas ich przechowywania.

4) EPR spectra of the analysed melanin are homogeneously broadened.
5) Continuous microwave saturation of EPR lines points out that slow spin-lattice relaxation processes characterize the melanin sample.
6) It is expected that free radicals of cosmetics containing melanin isolated from Sepia officinalis indicate toxic effects in human tissues.
7) It is possible that melanin's free radicals interactions with oxygen molecules O_2 destroy cosmetics during storage.

Piśmiennictwo

[1] Sarna T., Badanie struktury i właściwości centrów aktywnych melanin, Zagadnienia Biofizyki Współczesnej 1981, 6, 201-219.
[2] Sealy R.C., Hyde J.S., Felix C.C., Menon I.A., Prota G., Eumelanins and pheomelanins: characterization by electron spin resonance spectroscopy. Science 1982, 217, 545-547.
[3] Pasenkiewicz-Gierula M., Badanie struktury i dynamiki paramagnetycznych układów molekularnych o spinie s = 1/2 metodą elektronowego rezonansu paramagnetycznego (ERP). Rozprawa habilitacyjna, Uniwersytet Jagielloński, Kraków 1990.
[4] Korytowski W., Jonowymienne właściwości melanin – oddziaływanie z jonami metali, Zeszyty Naukowe Uniwersytetu Jagiellońskiego 1982, 9, 279-283.
[5] Krzywda A., Petelenz E., Michalczyk D., Płonka P.M., Sclerotia of the acellular (true) slime mould Fuligo septica as a model to study melanization and anabiosis, Cell Molecular Biology letters 2008, 13, 130-143.
[6] Okazaki M., Kuwata K., Miki Y., Shiga S., Shiga T., Electron spin relaxation of synthetic melanin and melanin – containing human tissues as studied by electron spin echo and electron spin resonance, Archives of Biochemistry and Biophysics 1985, 242, 197-2005.
[7] Buszman E., Pilawa B., Zdybel M., Wilczyński S., Gondzik A., Witoszyńska T., Wilczok T., EPR examination of Zn^{2+} and Cu^{2+} binding by pigmented soil fungi Cladosporium cladosporioides, Science of the Total Environment 2006, 363, 195-205.
[8] Matuszczyk M., Buszman E., Pilawa B., Witoszyńska T., Wilczok T., Cd^{2+} effect on free radicals in Cladosporium cladosporioides – melanin tested by EPR spectroscopy, Chemical Physics Letters 2004, 394, 366-371.
[9] Pilawa B., Buszman, E., Gondzik A., Wilczyński S., Zdybel M., Witoszyńska T., Wilczok T. Effect of pH on paramagnetic centers in Cladosporium cladosporioides, Acta Physica Polonica A 2005, 108, 147-150.
[10] Pilawa B., Latocha M., Krzyminiewski R., Kruczyński Z., Buszman E., Wilczok T., Effect of temperature on melanin EPR spectra, Physica Medica 2004, XX(Suppl. 1), 96-98.
[11] Pilawa B., Chodurek E., Wilczok T., Types of paramagnetic centres in Cu^{2+} complexes with model neuromelanins, Applied Magnetic Resonance 2003, 24, 417-422.
[12] Chodurek E., Pilawa B. , Dzierżęga-Lęcznar A., Kurkiewicz S., Świątkowska L., Wilczok T., Effect of Cu^{2+} and Zn^{2+} ions on DOPA-melanin structure as analyzed by pyrolysis-gas chromatography-mass spectrometry and EPR spectroscopy, Journal of Analytical and Applied Pyrolysis 2003, 70, 43-54.

References

[13] Buszman E., Pilawa B., Zdybel M., Wrześniok D., Grzegorczyk A., Wilczok T., EPR examination of Zn^{2+} and Cu^{2+} effect on free radicals in DOPA-melanin-netilmicin complexes, Chemical Physics Letters 2005, 403, 22-28.
[14] Buszman E., Pilawa B., Zdybel M., Wrześniok D., Grzegorczyk A., Wilczok T., Paramagnetic centers in DOPA-melanin-dihydrostreptomycin complexes, Acta Physica Polonica A 2005, 108, 353-356.
[15] Pilawa B., Latocha M., Buszman E., Wilczok T., Effect of oxygen on spin-spin and spin-lattice relaxation in DOPA-melanin. Complexes with chloroquine and metal ions, Applied Magnetic Resonance 2003, 25, 105-111.
[16] Pilawa B., Buszman E., Wrześniok D., Latocha M., Wilczok T., Application of EPR spectroscopy to examination of gentamicin and kanamycin binding to DOPA-melanin, Applied Magnetic Resonance 2002, 23, 181-192.
[17] Duliu O. G., Electron paramagnetic resonance identification of irradiated cuttlefish (Sepia officinalis L.), Applied Radiation and isotopes 2000, 52, 1385-1390.
[18] Bartosz G., Druga twarz tlenu. Wolne rodniki w przyrodzie, Warszawa, PWN 2006.
[19] Eaton G.R., Eaton S.S., Salikhov K.M. (eds), Foundations of modern EPR, World Scientific, Singapore, New Jersey, London, Hong Kong 1998.
[20] Baumann L., Cosmetic dermatology 2002.
[21] Gibka J., Wykorzystanie melaniny i procesu melanogenezy w kosmetyce, Polish Journal of Cosmetology 2000, 3, 164-176.
[22] Stankowski J., Hilczer W., Pierwszy krok ku spektroskopii rezonansów magnetycznych, Ośrodek Wydawnictw Naukowych PWN 2006.
[23] Wertz J. E., Bolton J. R., Electron Spin Resonance. Elementary Theory and Practical Applications, New York, London, 1986.
[24] Kozdrowska L., Właściwości centrów paramagnetycznych kompleksów DOPA-melaniny z kanamycyną i jonami miedzi (II), Rozprawa doktorska, Uniwersytet Zielonogórski, Zielona Góra 2005.
[25] Zdybel M., Złożony układ centrów paramagnetycznych kompleksów DOPA-melaniny z netilmicyną, jonami cynku(II) i miedzi(II), Rozprawa doktorska, Śląski Uniwersytet Medyczny, Katowice 2008.
[26] Pilawa B., Zdybel M., Latocha M. , Krzyminiewski R., Kruczyński Z., Analysis of lineshape of black Drosophila melanogaster EPR spectra, Current Topics of Biophysics 2008, 31, 5-9.